CRYOGENIC SYSTEMS AND SUPERCONDUCTIVE POWER

B. D. Hatch, et al

General Electric Corporate Research and Development

Prepared for:

Advanced Research Projects Agency

16 July 1974

Unclassified

SECURITY CLASSIFICATION OF THIS PAGE *(When Dete Entered)*

REPORT DOCUMENTATION PAGE		READ INSTRUCTIONS BEFORE COMPLETING FORM
1. REPORT NUMBER SRD-74-080	2. GOVT ACCESSION NO.	3. RECIPIENT'S CATALOG NUMBER AD 786 156
4. TITLE *(and Subtitle)* CRYOGENIC SYSTEMS AND SUPERCONDUCTIVE POWER, Phase III Final Technical Report		5. TYPE OF REPORT & PERIOD COVERED Final, 1 Oct 1973 to 16 July 1974 6. PERFORMING ORG. REPORT NUMBER
7. AUTHOR(s) B. D. Hatch, J. D. Hurley, D. W. Jones, and E. T. Laskaris		8. CONTRACT OR GRANT NUMBER(s) DAHC-15-72-C-0235
9. PERFORMING ORGANIZATION NAME AND ADDRESS Corporate Research and Development General Electric Company Schenectady, New York 12301		10. PROGRAM ELEMENT, PROJECT, TASK AREA & WORK UNIT NUMBERS ARPA Order No. 2200 Amend. 2, PC 4D10
11. CONTROLLING OFFICE NAME AND ADDRESS Department of Defense Advanced Research Projects Agency Arlington, Virginia 22209		12. REPORT DATE 16 July 1974 13. NUMBER OF PAGES 90
14. MONITORING AGENCY NAME & ADDRESS *(if different from Controlling Office)*		15. SECURITY CLASS. *(of this report)* Unclassified 15a. DECLASSIFICATION/DOWNGRADING SCHEDULE

16. DISTRIBUTION STATEMENT *(of this Report)*

Approved for public release - distribution unlimited.

17. DISTRIBUTION STATEMENT *(of the abstract entered in Block 20, if different from Report)*

18. SUPPLEMENTARY NOTES

19. KEY WORDS *(Continue on reverse side if necessary and identify by block number)*

Cryogenic
Superconductive
Liquid metal
Propulsion
Electrical
Machinery

20. ABSTRACT *(Continue on reverse side if necessary and identify by block number)*

Extreme environments are a common requirement of military applications of propulsion machinery. It is essential that superconductive propulsion systems for ships and military vehicles be of rugged and highly reliable construction. For this reason, dominant emphasis has been given during Phase III to shock and vibration testing of representative superconductive coils while operating in a superconducting mode near the upper current density limit. Supplementary tests have also been made to determine structural and mechanical

DD FORM 1 JAN 73 1473 EDITION OF 1 NOV 65 IS OBSOLETE

Unclassified

SECURITY CLASSIFICATION OF THIS PAGE *(When Data Entered)*

Short Title of Work	CRYOGENIC SYSTEMS AND SUPERCONDUCTIVE POWER
Contract No.	DAHC-15-72-C-0235
ARPA Order No.	2200 Amendment No. 2, Program Code 4D10
Contractor	Cryogenics Branch Power Generation and Propulsion Laboratory Corporate Research and Development General Electric Company P.O. Box 43 Schenectady, New York 12301
Principal Investigator	B. D. Hatch
Project Scientists	R. B. Fleming D. W. Jones E. T. Laskaris D. L. Kerr S. H. Minnich
Effective Date of Contract	1 June 1972
Contract Expiration Date	16 July 1974
Amount of Contract	$705,997

20. ABSTRACT (cont'd)

properties of materials applicable to the composite material of the superconductive coil while at liquid helium temperatures. The second area of experimental evaluation conducted during Phase III involved liquid metal collectors for acyclic superconductive machines in which gallium is used as the liquid metal. These tests have been conducted to identify potential materials and process problem areas and to demonstrate the potential resolution of such problems.

FOREWORD

This Phase III final technical report was prepared by Corporate Research and Development of the General Electric Company in Schenectady, New York, under Advanced Research Projects Agency Contract No. DAHC-15-72-C-0235, "Cryogenic Systems and Superconductive Power," ARPA Order No. 2200. This contract is administered by General Electric Corporate Research and Development for the Department of Defense, Advanced Research Projects Agency, Washington, D. C.

The engineering development work reported covers the period from 1 October 1973 to 16 July 1974. This work is under the direction of Mr. B. D. Hatch, Principal Investigator.

ABSTRACT

Extreme environments are a common requirement of military applications of propulsion machinery. It is essential that superconductive propulsion systems for ships and military vehicles be of rugged and highly reliable construction. For this reason, dominant emphasis has been given during Phase III to shock and vibration testing of representative superconductive coils while operating in a superconducting mode near the upper current density limit. Supplementary tests have also been made to determine the structural and mechanical properties of materials applicable to the composite material of the superconductive coil while at liquid helium temperatures.

The second area of experimental evaluation conducted during Phase III involved liquid metal collectors for acyclic superconductive machines in which gallium is used as the liquid metal. These tests have been conducted to identify potential materials and process problem areas and to demonstrate the potential resolution of such problems.

TABLE OF CONTENTS

TABLE OF CONTENTS (Cont'd)

LIST OF ILLUSTRATIONS

LIST OF ILLUSTRATIONS (Cont'd)

LIST OF ILLUSTRATIONS (Cont'd)

LIST OF ILLUSTRATIONS (Cont'd)

LIST OF TABLES

LIST OF TABLES (Cont'd)

Section 1

SUMMARY

TECHNICAL PROBLEM

Two principal problem areas related to the materials and processes associated with the practical application of superconductivity to power and propulsion systems for the Department of Defense have been investigated experimentally during Phase III of this study contract. The first area is that of demonstrating that superconducting coils can be constructed using available materials, processes, and assembly methods and that when so constructed and assembled they will perform satisfactorily under the extremes of shock and vibration environment encountered in military applications. The second problem area is that of demonstrating that liquid metal current collectors for acyclic superconductive machinery can be built using available materials and processes with gallium and that such collectors may be expected to perform satisfactorily in military applications.

METHODOLOGY

The work was divided into the two principal task areas, and project engineers and personnel were assigned to each area. The designs for test specimens and special test equipment had been prepared during Phase II, and parts for their assembly had been fabricated. These parts were assembled and tested during Phase III; they were supplemented and modified during the course of assembly and test.

SUPERCONDUCTIVE COIL TECHNOLOGY

As reported in many literature sources, an instantaneous relative motion between the superconducting coil and its support or between one segment of the superconducting coil and another can cause sufficient frictional heating to raise the temperature of the coil locally above the critical temperature of the superconductor. When raised above its critical temperature, the superconducting material suddenly changes from its superconducting state (i.e., having essentially no measurable electrical resistance) into a normal, resistive state (i.e., having resistance considerably higher than that of copper or other commonly used electrical conductor materials).

The very high electrical currents carried by the superconductor (e.g., 15,000 A/cm^2) must suddenly be carried by a normally resistive wire, with the result that the resistive heating rapidly raises the temperature further. The high magnetic field of the superconducting coil collapses. To restore its usefulness, all power must be removed from the coil, and the coil must again be cooled to the very low cryogenic temperatures below the critical temperature

at which the material is superconductive. Power may then be applied to restore the magnetic field of the superconducting coil(s) and return the motor or generator (or other device) to useful service.

The specific objective of this portion of Phase III has been to demonstrate that the materials and processes by which the specimen superconducting coils were built* during Phase II when these coils were mounted and tested in a configuration suitable for application to acyclic machinery did result in such satisfactory performance as to clearly indicate that military applications of superconductive machinery would be successful and reliable.

Very favorable and satisfactory results were obtained. The superconducting coils were subjected to peak transverse shock accelerations of 700 g (i.e., 700 times the force of gravity) and to sustained shocks (i.e., for periods of 2 ms or more) of 110 g while operating in its superconductive mode at high current densities very near (equal to 96 percent of) the critical current without any failure.

In the axial direction the shock threshold was at 260 g. These tests were performed repeatedly in all major axes, in both torsional and translation modes. In all instances it required peak and sustained shock forces greater than these values, to cause a coil to go normal After such an occurrence, the coil assembly was again cooled below the critical temperature, and the full rated superconducting performance of the coil was obtained.

The superconducting coils were also subjected to linear vibration at variable frequencies between 1000 and 3000 cpm, with peak accelerations up to 30 g, with superconducting coil current densities at 97 percent of the critical current. The coils remained superconducting under all of the conditions of these tests. Torsional vibration was applied over the range of 500 to 3800 cpm, with peak torsional accelerations (at the outside radius of the coil) of 13.5 g, with the coil current densities at 98 percent of the critical current. The coils remained superconducting under all of the conditions of these tests. More severe testing was limited by the test equipment available for these tests.

These tests are considered to have fully demonstrated, to the maximum level of confidence possible with this number of experimental test specimens and the repeated tests of them, that superconducting coils produced with the tested materials, processes, and mounting provisions will perform fully satisfactorily in ship propulsion applications. It also indicates that fully satisfactory performance of superconducting coils may be expected in most other military applications.

It is of course recognized that potential applications of superconducting coils exist in which the range of vibration frequency or of shock intensity will

*These impregnated niobium-titanium coils were supplied by the General Electric Company.

exceed those covered by these tests. It is also recognized that each superconducting coil application will have its own coil configurations, mountings, and dimensions, thus requiring its own tests to demonstrate its satisfactory application.

These Phase III tests do provide confidence in the ability to design and build satisfactory superconductive coils for military applications.

LIQUID METAL CURRENT COLLECTOR STUDIES

The main purpose of this task was to design, construct, and test an unflooded electrical current collection system using gallium as the liquid metal. Most of the previously successful work pertaining to current collection systems for superconductive acyclic machines has involved the use of a sodium-potassium alloy, NaK.

NaK has the advantages of excellent compatibility with many commonly used materials in electrical machinery design (including copper and iron), low viscosity, low density, and good electrical conductivity. The outstanding disadvantage of NaK is its highly reactive nature when in contact with oxygen, water, and a number of other common substances, including fluoropolymers.

Gallium, on the other hand, is a low-hazard material, being nontoxic, nonreactive to water, and substantially nonreactive to oxygen, due to the formation of a protective oxide that instantaneously forms on the gallium.

Any liquid metal surface oxidizes instantaneously, and when flowing in a liquid (e.g., molten) state, it must be protected from oxygen if the cumulative formation of oxides is to be prevented. Thus any liquid metal collector system that is to operate satisfactorily over any extended period of time must be enclosed in an inert gas atmosphere, so oxygen may be effectively excluded. This is applicable to gallium, NaK, or any of the various other low-melting-point metals and alloys that might be considered for such an application. Of all such metals, gallium and NaK are the most promising.

GALLIUM COLLECTOR TEST RESULTS

Developmental systems have been successfully operated for hundreds of hours at surface speeds exceeding 5000 ft/min by other investigators using an oxygen-free cover gas. The tests during Phase III included an approximately 90-day period of testing activity using gallium as the liquid metal with a nitrogen cover gas obtained from liquid nitrogen. The oxygen content of this gas was measured to be in the range of 9 to 12 ppm. Because the saturation pressure of water vapor at liquid nitrogen temperature is approximately 10^{-17} torr, the water vapor in the nitrogen gas immediately above the liquid surface would be well below 1 ppm.

The apparatus was designed to minimize oxygen and water vapor penetration by diffusion. It was pumped down to a vacuum of less than 100 micron pressure and was back filled with the cover gas several times before the system was filled with gallium.

During the 90-day testing period, the test assembly was opened up and the liquid metal was exposed to the atmosphere a number of times. It was also disassembled and reassembled. Approximately 45 hours of testing during the test period consisted of rotating collector tests, of which about 35 hours were under high-intensity magnetic fields inside an energized superconductive coil. The axis of rotation during these tests was inclined to simulate the pitch of a ship propellor shaft.

A filtering system for the liquid gallium was designed and incorporated in the test equipment. A fraction of the liquid gallium passed through this filter. Some tests were run with the filtering loop closed by valves. At no time during the test period was any difficulty experienced in the mechanical or electrical operation of the gallium liquid metal collectors, due to the formation of gallium oxides (i. e., the reported black powders, sludging, etc. representative of some earlier experiments using gallium).

It should be noted that this black powder consisted of very small (macroscopic and microscopic) spheres of gallium enclosed in thin shells of gallium oxide. This powder was sufficiently fine to be moved by the turbulent flow of the nitrogen cover gas into far corners and onto various free surfaces of the collector enclosure. The surfaces of a plastic insulating ring approximately 3/8 inch thick were coated with dust. The surface breakdown strength of this coated surface was measured to be in excess of 5000 V/in. There was no indication of any difficulty of any kind due to this dusting; very extended test times would have been required to determine the long-term effects of this powder.

The materials and processes used in the construction of these liquid metal collectors were demonstrated to be very satisfactory. The seals at the rotating shaft and elsewhere in the system performed very well, with no evidence of any wear or leakage. The configuration of the collector face(s) and of the gutters incorporated in the stator for the retention of the liquid metal in the location of the collector site was not fully effective. The liquid metal originally placed in the collector was not all retained in the collector site over the full period of the test.

The results of the tests with gallium demonstrate that there are no apparent materials compatibility problems and that gallium current collectors can be designed using stainless steel cladding in conjunction with a pure nitrogen cover gas system. Additional work is required in the areas of geometric and fluid dynamics designs of the collector, to ensure containment of the liquid metal in the desired areas. This additional work is relevant to any liquid metal.

Section 2

SUPERCONDUCTING COIL TECHNOLOGY

SUPERCONDUCTING COIL SHOCK AND VIBRATION TESTS

The present experimental investigation aims at evaluating the performance of cylindrical superconducting coils and their supports in the presence of externally applied impact and vibratory forces and torques. As reported in many literature sources. an instantaneous relative motion between the coil and its support or between conductors within the coil can cause sufficient frictional heating to raise the temperature of the coil locally above the critical temperature of the superconductor and consequently result in quenching. Thus the coil supports should be designed to prevent such differential coil movements when external impact and vibratory forces and torques are applied to the support structure.

The specific objective of this investigation is to determine whether the extreme conditions of environmental shocks and vibrations that could be transmitted through the winding support structure might cause sufficient relative motion between coils and supports or between conductors to degrade the coil performance. The test apparatus setup for linear and torsional shock tests is shown in Figures 1 through 4. The linear and torsional vibrations are excited by the motor drive vibrator exciter, assembled as shown in Figures 5 and 6.

COIL MOUNTING POSITIONS

Two cylindrical coils (6.25-inch outer diameter by 3.0-inch inner diameter by 2.5-inch length), one made of copper wire and the other of superconductor wire, can be mounted on the support structure in such a manner that their principal axis could either be vertical or horizontal. In either position, the coils are spaced from each other and from the support plates by Textolite® disks that provide cooling and axial alignment of the coils (Figure 7). Twelve radial grooves 1/16 inch deep by 1/4 inch wide are machined at the faces of each disk, to allow for direct cooling by pool boiling of helium at the coil surfaces.

In their horizontal position (Figures 1 and 8) the coils are held flat against support plate P by square aluminum plate A, which is fastened directly to plate P by four 1/2-inch stainless steel bolts. The overall assembly of coils, leads, and supports is displayed in Figure 9.

The coils, mounted at their vertical position (Figures 2 and 10) are held flat against each other by two rectangular aluminum plates, S, and four 1/2-

®Trademark of the General Electric Company

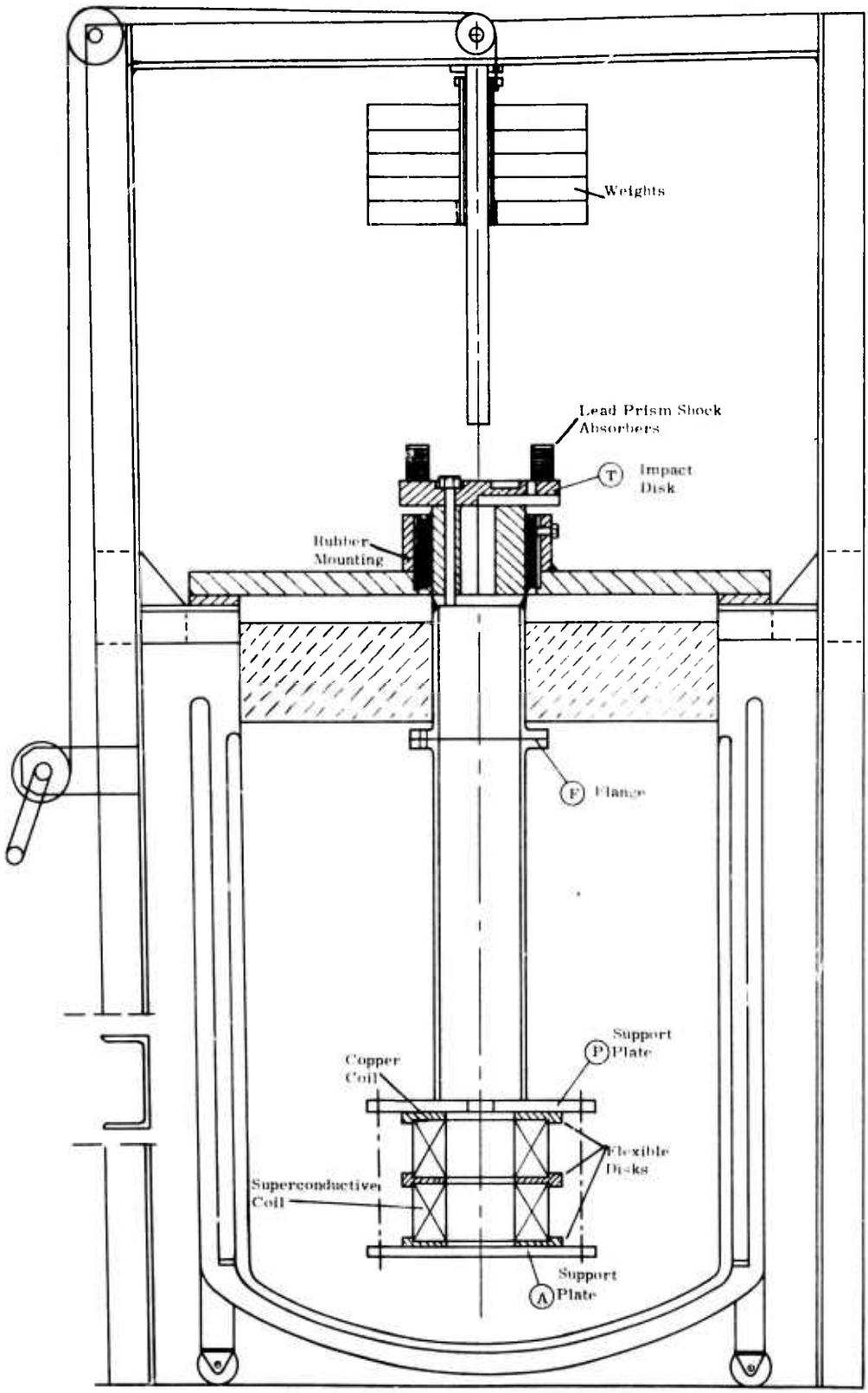

Figure 1. Apparatus Setup for Linear Shock Test Applications

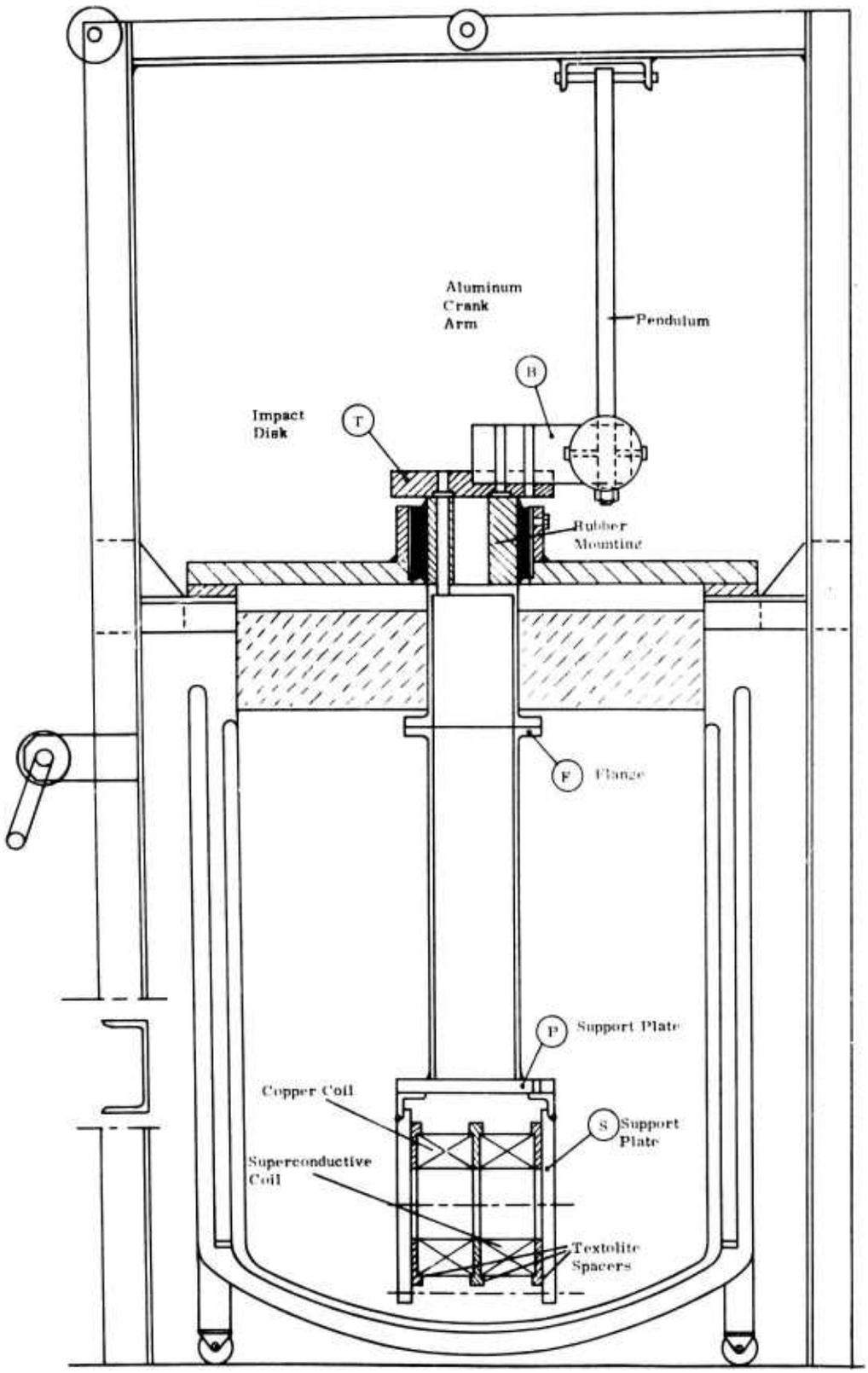

Figure 2. Apparatus Setup for Torsional Shock Test Applications

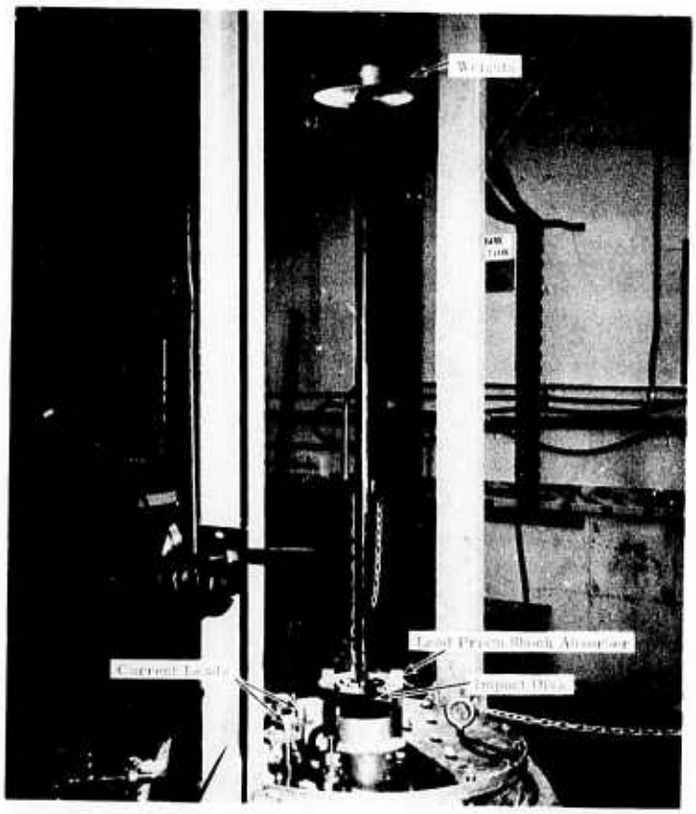

Figure 3. Test Apparatus for Exciting Linear Shocks

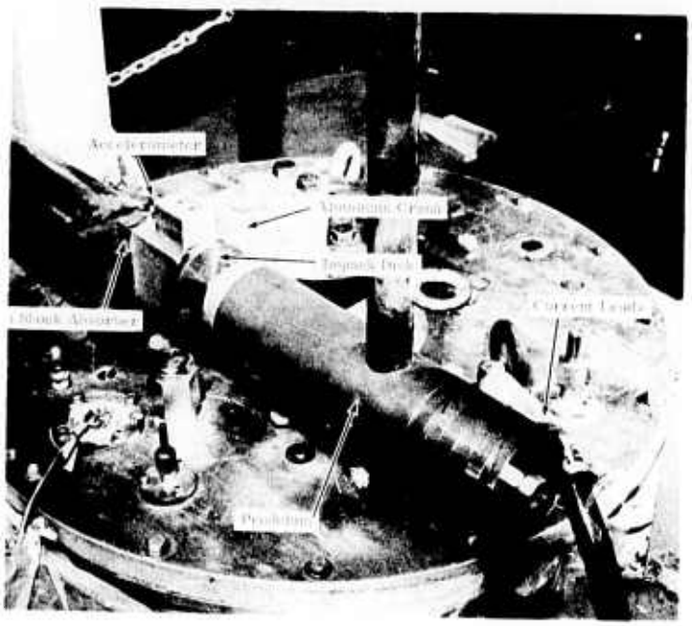

Figure 4. Test Apparatus for Exciting Torsional Shocks

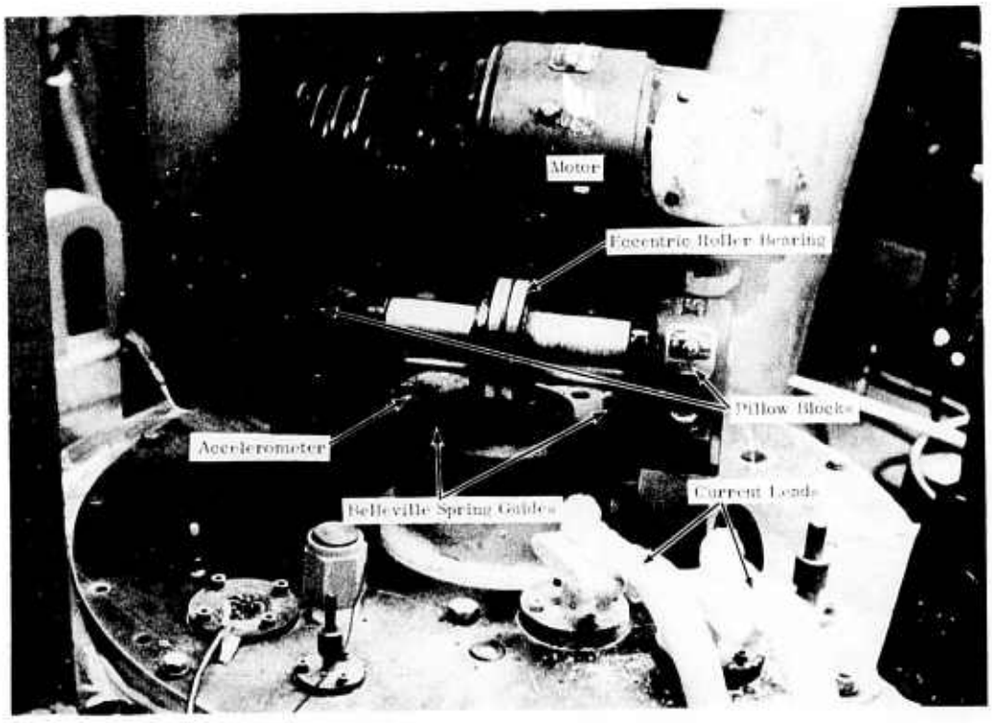

Figure 5. Vibrator Assembly for Linear Vibration Applications

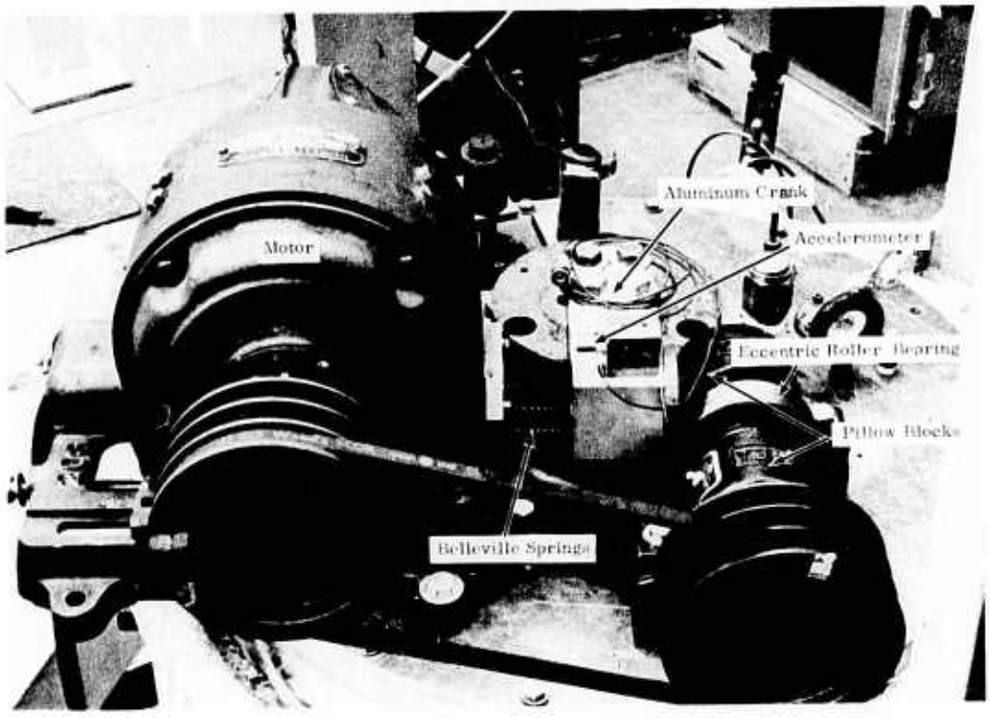

Figure 6. Vibrator Assembly for Torsional Vibration Applications

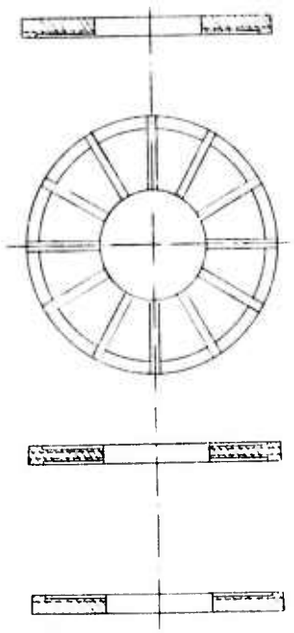

Figure 7. Textolite Disks for Coil Alignment and Cooling

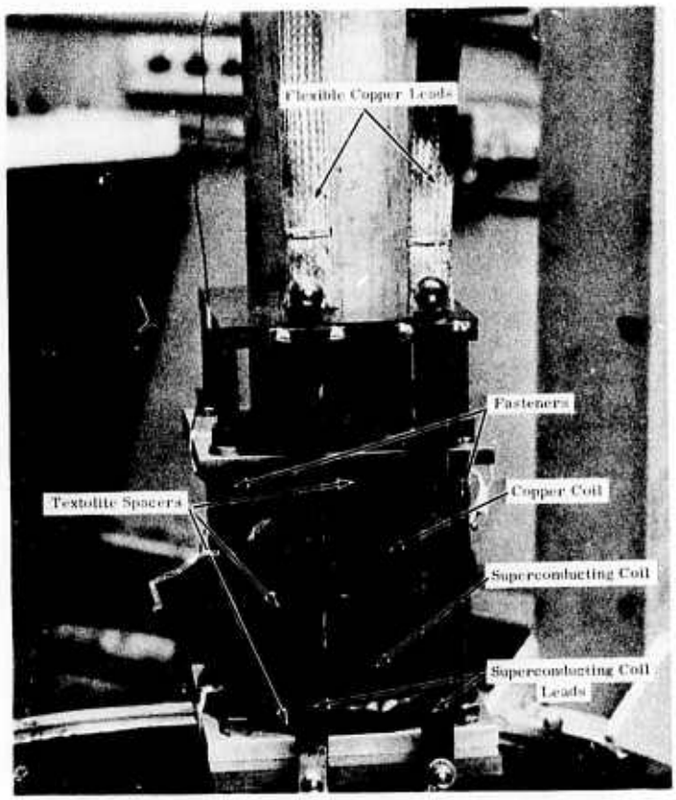

Figure 8. Coil Assembly with Principal Axis Vertical

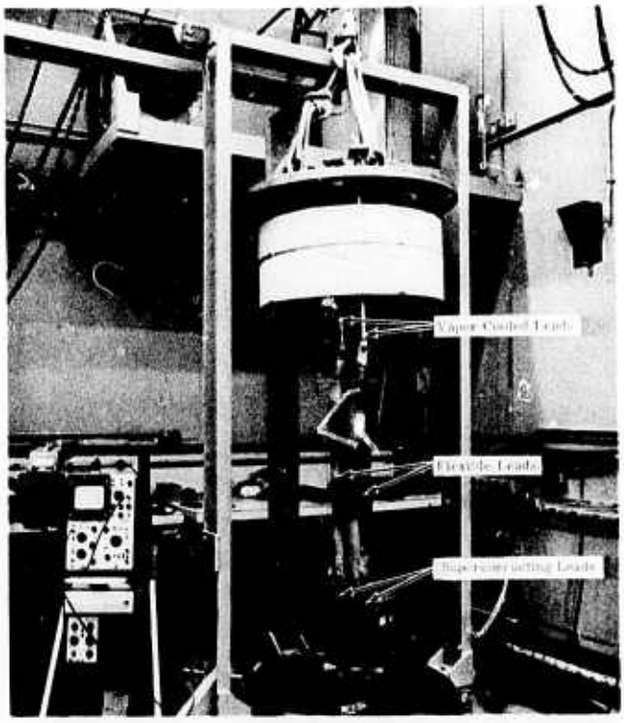

Figure 9. Overall Assembly of Coils, Leads, and Supports with Coil Axis Vertical

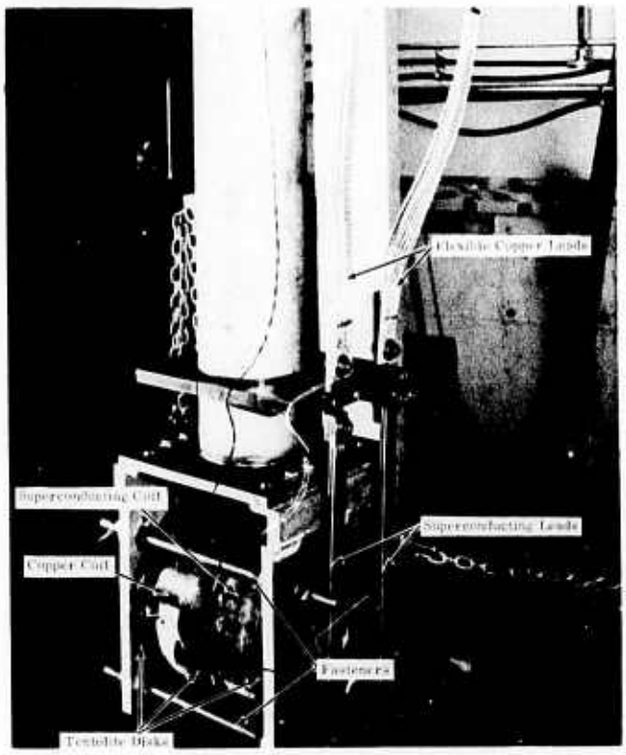

Figure 10. Coil Assembly with Principal Axis Horizontal

inch stainless steel bolts, B. The bolted assembly of coils and plates, S, is fastened to support plate P, as shown in Figure 2.

To fasten the stainless steel bolts, C, the assembly of coils and supports is cooled to 80°K and a torque of 600 in.-lb_f is applied. The corresponding load per bolt is 5600 lb_f, which yields a compressive stress of 950 psi between the coils and the supports.

The superconducting coil is wound of 0.050-inch-diameter niobium-titanium multifilament superconductor wire (360 filaments of superconductor with a copper-to-superconductor ratio of 1.25) manufactured by the Magnetic Corporation of America. The winding consists of 1488 turns arranged in 32 layers. Around each layer of the winding a complete turn of glass woven fabric is applied as interlayer insulation. The wound coil is impregnated by epoxy, making use of a vacuum controlled process to prevent the formation of air bubbles in the winding composite.

A series of electrical tests was performed on the coil to determine its critical current. The coil in these tests was simply supported between two parallel Textolite disks at a low clamping force and was cooled gradually to 4.2°K. The coil was then energized at a constant voltage of 0.2 volt until it quenched and the critical current was measured. The data that were obtained from a series of tests indicate that the coil does not experience any training and quenches consistently at a critical current of 455 amperes.

As displayed in Figures 1 through 6, the linear shock and vibratory forces were always applied in a vertical direction, while the torsional shocks and vibrations were always excited about a vertical axis. To absorb the impact due to the linear and torsional shock, lead prism shock absorbers (1 x 1 x 0.525 inch) were employed as shown in Figures 3 and 4. The number and position of these prisms was varied to vary the magnitude of the shock acceleration.

RESULTS AND CONCLUSIONS

The results of the present investigation can be summarized as follows:

Category	Results
Linear shock tests, coil axis vertical	The superconducting coil, energized to currents up to 400 amperes (88 percent of its critical current), remains superconductive when it is subjected to peak accelerations up to 1700 g or average accelerations up to 260 g for shock durations up to 2.2 ms. At peak accelerations exceeding 1800 g or average accelerations above 330 g, the superconducting coil quenches con-

Category	Results
	sistently for currents of 350 amperes and above.
Linear shock tests, coil axis horizontal	The coil performance is not affected for currents up to 440 amperes (97 percent of its critical current) when it is subjected to linear shocks of 700-g peak acceleration or 112-g average acceleration for shock durations up to 3.2 ms.
	The superconducting coil energized to currents of 300 amperes and above quenches when it is subjected to peak accelerations in excess of 770 g or average accelerations of 160 g and above.
Torsional shock tests, coil axis vertical	The coil remains superconductive at currents up to 97 percent of its critical current when it is subjected to linear accelerations at its outer diameter of peak value up to 1700 g and average value up to 470 g for shock duration up to 3 ms.
Torsional shock tests, coil axis horizontal	The coil, energized to currents up to 445 amperes (98 percent of its critical current) remains superconductive when subjected to torsional impacts that yield linear acceleration at its outer diameter of peak value up to 2570 g, average value up to 530 g, and time duration up to 1.5 ms.
Linear vibration tests, coil axis vertical	The coil was subjected to linear vibration of 0.060-inch double amplitude, variable frequency from 1000 to 3000 cpm, peak accelerations up to 30 g, and currents up to 440 amperes. The coil did not quench under any of these conditions.
Linear vibration tests, coil axis horizontal	The coil was energized at currents up to 451 amperes and was subjected to linear vibration of 0.060-inch double amplitude, variable frequency from 920 to 3300 cpm, and peak accelerations up to 40 g with no effect on its performance.

Category	Results
Torsional vibration tests, coil axis vertical	The superconducting coil, energized to currents up to 448 amperes, was subjected to torsional vibration of 0.00857-radian double amplitude, variable frequency from 500 to 3840 cpm, and peak linear acceleration at its outer diameter up to 13.5 g. The coil remained superconductive in all cases.
Torsional vibration tests, coil axis horizontal	The superconducting coil, energized to currents up to 445 amperes, was vibrated torsionally at a constant amplitude of 0.00817-radian double amplitude, variable frequency from 500 to 3800 cpm, and peak acceleration up to 13 g at its outer diameter. No effect on the coil performance was observed.

The test results indicate further that for all practical purposes the coil performance under the influence of applied linear shocks does not depend on the current, while it is strongly dependent upon the acceleration. Clearly this behavior can be attributed to the relative motion between the coil and its support during the impact, which can generate sufficient local heating to raise the temperature of the coil locally above the critical temperature of the superconductor.

To assess the relative importance of coil impregnation versus the method of support, the test results for the case of linear shock accelerations in the direction of the coil axis can be compared with the results for the case of linear shock accelerations normal to the coil principal axis. In the former case, the relative motion between the coil and its support is greatly restricted and the superior performance can be attributed to the impregnation technique. The latter case, however, favors the coil support motion and the inferior performance experienced well justifies the importance of tight coil supports.

INSTRUMENTATION

The acceleration measurements were performend using a piezoelectric acceleration transducer, model 2213C, serial no. LB37, manufactured by the Endevco Corporation. Because the output impedance of the piezoelectric transducer is much higher than that which most electronic measuring systems would require, a high-impedance operational amplifier, model P501A/B/C, manufactured by Analog Devices, Inc., was used to provide high (over 100 MΩ) impedance between the accelerometer and the readout instrumentation. At high accelerations, the output voltage of the transducer may be sufficiently high in amplitude to saturate the amplifier (saturation voltage is ± 10 volts).

To reduce the transducer output signal a capacitance shunt was connected in parallel and the reduced signal was fed to the amplifier. The added capacitance would reduce the sensitivity of the accelerometer according to the relation:

$$E = E_c \frac{(C_p + 100)}{(C_p + C_t)} \text{ rms mV/single peak g} \qquad (1)$$

where:

E_c = Factory supplied calibration sensitivity in rms mV/single peak g, calibrated with 100-mmfd external capacitance

E = Actual sensitivity for any total external capacitive loading C_e on the accelerometer

C_p = Accelerometer capacitance alone in mmfd (supplied by the factory)

C_t = Total externally applied capacitance in mmfd

The test accelerometer was calibrated dynamically relative to a piezoelectric standard accelerometer (model 2215C, serial no. KB35), manufactured by the Endevco Corporation. The comparison calibration was performed by mounting the test transducer and the reference transducer back-to-back (Figure 11) on the table of the electromagnetic vibration exciter, as shown in Figure 12.

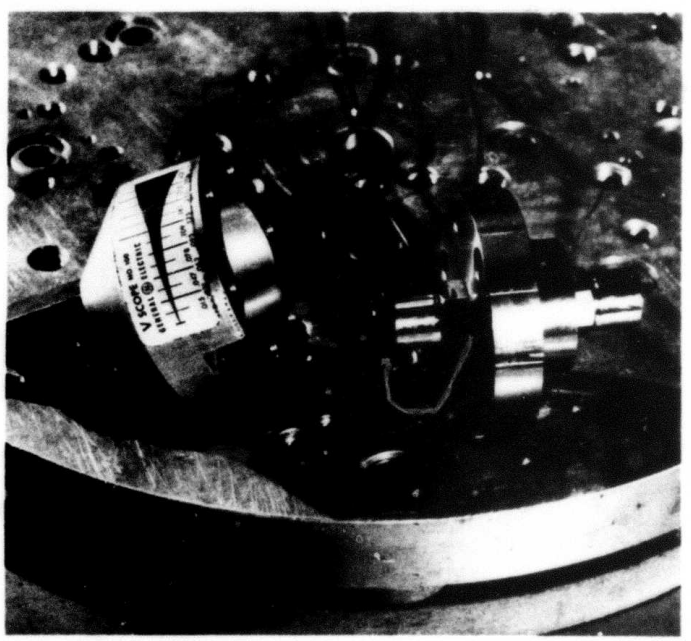

Figure 11. Test Accelerometer Mounted Back-to-Back with Standard Accelerometer for Dynamic Calibration

Figure 12. Dynamic Calibration of Test Accelerometer Versus Standard Accelerometer, Performed on Electromagnetic Vibration Exciter

The output voltages of each accelerometer were measured on a Ballantine true rms voltmeter (model 323-01) and they were recorded on a Tektronix storage oscilloscope (type 564). The calibration tests were conducted as follows:

- The frequency of the vibrator was held constant while the acceleration was set according to the output readings of the standard accelerometer. The output voltage of the test accelerometer was measured (Table 1) and recorded as displayed in Figure 13.
- The frequency of the vibrator was varied while the acceleration or the output voltage of the standard accelerometer was held constant. The output voltage of the test accelerometer was measured (Table 1) and recorded in Figure 14.
- A shunt capacitance of 0.0033 mFd was connected in parallel to the test accelerometer, to reduce the signal by a factor of four. The reduced output voltage is given in Table 1 and Figure 15.

As a result of the calibration tests, the sensitivity of the test accelerometer was determined for the range of frequencies from 100 to 3000 hertz and accelerations from 1 to 40 g, with accuracy of 1 percent; therefore, test accelerometer sensitivity = 21.4 g/V.

Table 1

CALIBRATION MEASUREMENTS OF TEST ACCELEROMETER VERSUS STANDARD ACCELEROMETER

Frequency (hertz)	Accelerations (g)	Standard Accelerometer (volts rms)	Test Accelerometer (volts rms)	Shunt Capacitance on Test Accelerometer (mFd)
100	1	0.00781	0.0329	None
100	2	0.0156	0.0662	None
100	5	0.0391	0.1620	None
100	10	0.0781	0.3300	None
100	15	0.1170	0.4970	None
100	20	0.1560	0.6620	None
100	40	0.3120	1.3200	None
200	5	0.0391	0.1610	None
400	5	0.0391	0.161	None
600	5	0.0391	0.161	None
800	5	0.0391	0.161	None
1000	5	0.0391	0.161	None
1500	5	0.0391	0.160	None
2000	5	0.0391	0.160	None
2500	5	0.0391	0.160	None
3000	5	0.0391	0.157	None
100	20	0.1560	0.160	0.0033
100	40	0.3120	0.320	0.0033
100	5	0.0391	0.040	0.0033
2000	5	0.0391	0.040	0.0033
3000	5	0.0391	0.040	0.0033

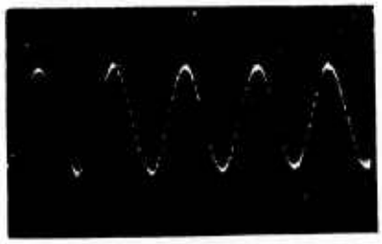

Test Accelerometer Output at 15-g Acceleration, 100-Hertz Frequency (Oscilloscope sensitivity is 0.5 V/cm vertically and 5 ms/cm horizontally.)

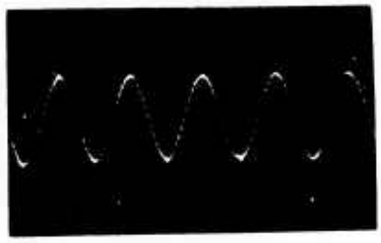

Test Accelerometer Output at 5-g Acceleration, 100-Hertz Frequency (Oscilloscope sensitivity is 0.2 V/cm vertically and 5 ms/cm horizontally.)

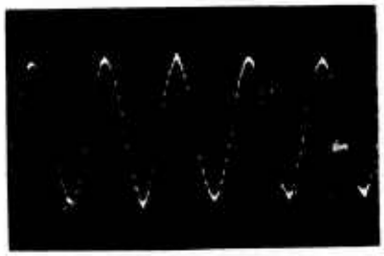

Test Accelerometer Output at 20-g Acceleration, 100-Hertz Frequency (Oscilloscope sensitivity is 0.5 V/cm vertically and 5 ms/cm horizontally.)

Test Accelerometer Output at 10-g Acceleration 100-Hertz Frequency (Oscilloscope sensitivity is 4.0 V/cm vertically and 5 ms/cm horizontally.)

Figure 13. Calibration of Test Accelerometer of Constant Frequency and Variable Acceleration

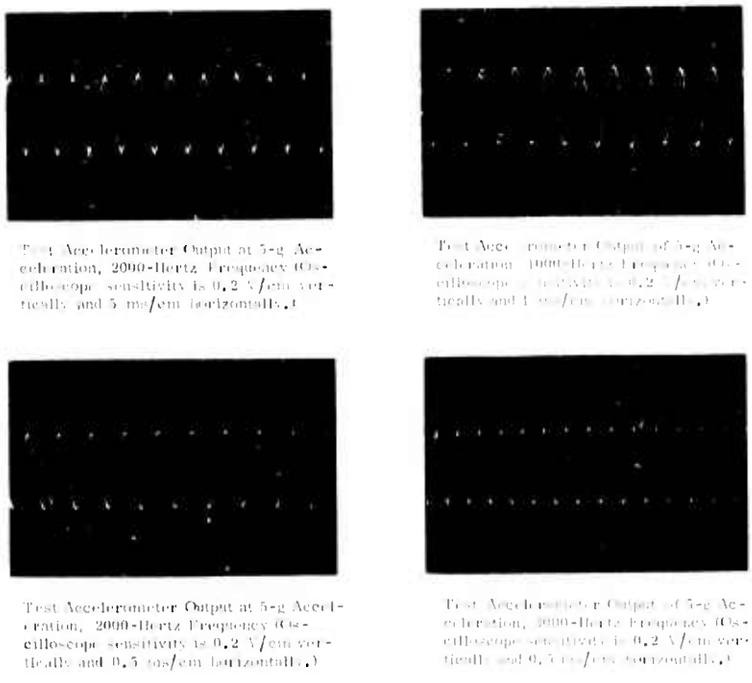

Test Accelerometer Output at 5-g Acceleration, 2000-Hertz Frequency (Oscilloscope sensitivity is 0.2 V/cm vertically and 5 ms/cm horizontally.)

Test Accelerometer Output at 5-g Acceleration, 1000-Hertz Frequency (Oscilloscope sensitivity is 0.2 V/cm vertically and 1 ms/cm horizontally.)

Test Accelerometer Output at 5-g Acceleration, 2000-Hertz Frequency (Oscilloscope sensitivity is 0.2 V/cm vertically and 0.5 ms/cm horizontally.)

Test Accelerometer Output at 5-g Acceleration, 3000-Hertz Frequency (Oscilloscope sensitivity is 0.2 V/cm vertically and 0.5 ms/cm horizontally.)

Figure 14. Calibration of Test Accelerometer of Constant Acceleration and Variable Frequency

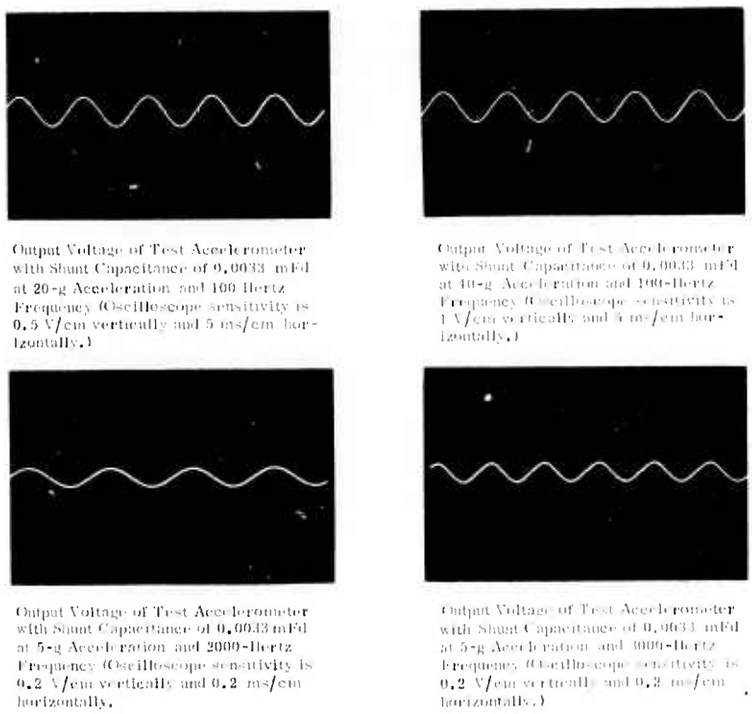

Output Voltage of Test Accelerometer with Shunt Capacitance of 0.0033 mFd at 20-g Acceleration and 100 Hertz Frequency (Oscilloscope sensitivity is 0.5 V/cm vertically and 5 ms/cm horizontally.)

Output Voltage of Test Accelerometer with Shunt Capacitance of 0.0033 mFd at 40-g Acceleration and 100-Hertz Frequency (Oscilloscope sensitivity is 1 V/cm vertically and 5 ms/cm horizontally.)

Output Voltage of Test Accelerometer with Shunt Capacitance of 0.0033 mFd at 5-g Acceleration and 2000-Hertz Frequency (Oscilloscope sensitivity is 0.2 V/cm vertically and 0.2 ms/cm horizontally.

Output Voltage of Test Accelerometer with Shunt Capacitance of 0.0033 mFd at 5-g Acceleration and 3000-Hertz Frequency (Oscilloscope sensitivity is 0.2 V/cm vertically and 0.2 ms/cm horizontally.)

Figure 15. Calibration of Test Accelerometer with Shunt Capacitance of 0.0033 mFd to Reduce Accelerometer Signal by Factor of Four

For the series of linear shock experiments, the accelerometer was mounted on th center of a 3/8-inch-thick plate (Figure 16), which was inserted between the cylindrical core of the rubber mounting and the top circular plate. The position of the accelerometer for the linear vibration tests is displayed in Figure 5, while Figures 4 and 6 show the accelerometer assembly for the torsional shock and vibration tests, respectively.

Figure 16. Accelerometer Assembly for Linear Shock Tests

The current through the superconducting coil was measured by using a Beede digital d-c millivoltmeter to measure the voltage drop across a 500-ampere, 50-mV shunt. The voltage across the superconducting coil terminals was monitored by a Keithley (model 160) digital voltmeter. The coil was energized by a d-c power supply (model SCR20-500) manufactured by Electronic Instruments, Inc.

PRELIMINARY SHOCK TESTS

A series of preliminary tests was conducted to determine the yield strength of the specific lead prisms that were to be employed for damping the impact in the shock experiments. At high rates of deformation generated by the impact, not only the material properties but also the geometry of the lead prisms would contribute to the resulting yield strength.

The test setup for such experiments simply consists of a rigid foundation and a cylindrical weight, which is guided by a vertical tube through its bore.

The weight is released from a predetermined height and strikes the lead prisms that are positioned symmetrically around the vertical tube in the rigid metal foundation.

The results of a series of tests conducted on lead specimens with a 1 x 1-inch cross section and a 1.5-inch height were reported In Reference 1. The average yield strength of these prisms was found to be nearly constant (4000 psi).

The tests were repeated using lead prisms 1 x 1 x 0.525 inch. The results are summarized in Table 2, and Figure 17 plots the average yield strength versus the plastic deformation.

Table 2

SHOCK TESTS ON LEAD PRISMS
(1 x 1 x 0.525 Inch)

Test	Prism Dimensions			Average Cross Section	Plastic Deform	Load	Load Stroke	Lead Prisms	Yield Strength
	Before Shock		After Shock						
	A (in^2)	L (in.)	L (in.)	Aav (in^2)	d (in.)	G (lb)	H (in.)	M	S (psi)
1	1	0.525	0.47825	1.0489	0.04675	24	52.75	4	6454.4
2	1	0.525	0.4854	1.04079	0.0396	24	52.75	5	6143
3	1	0.525	0.4657	1.06367	0.0593	24	52.75	3	6690
4	1	0.525	0.4420	1.0939	0.083	24	52.75	2	6970
5	1	0.525	0.48975	1.03598	0.03525	24	52.75	6	5778
6	1	0.525	0.4967	1.02849	0.02828	24	52.75	7	6216
7	0.525	1.000	0.8235	1.1071	0.1765	23	45.25	2	5073
8	0.525	1.000	0.8750	1.1071	0.1250	23	45.25	3	4934
9	0.525	1.000	0.903	1.0837	0.097	23	45.25	4	4849

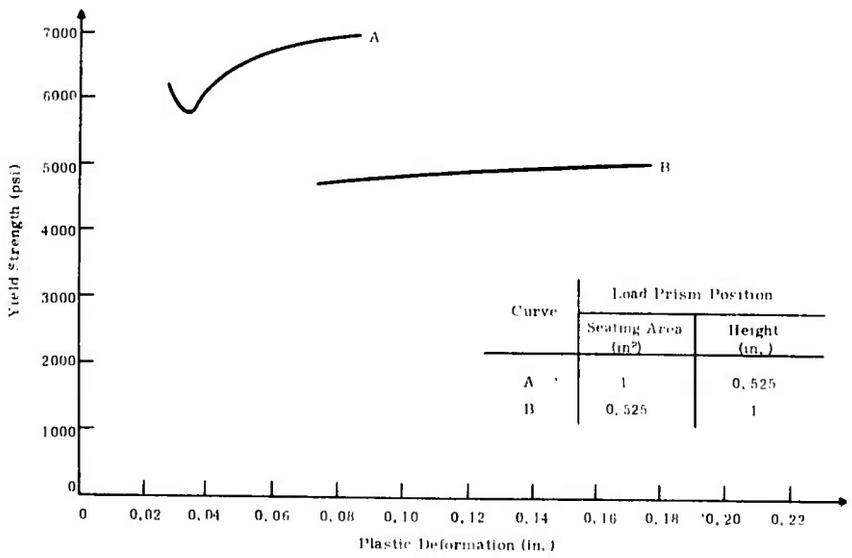

Figure 17. Average Yield Strength Versus Deformation for Lead Prisms (1 x 1 x 0.525 inch)

The difference between the yield strength of the 0. 525-inch prisms relative to the 1. 5-inch prisms is attributed to the difference in height and specifically to the difference in the unconstrained lateral area that is available for material flow.

The shock tests of the superconducting coil were performed using the lead prisms of 0. 525-inch height. The mass of the coil assemblies and their support structure are summarized in Table 3.

Table 3

MASS OF COIL ASSEMBLY AND SUPPORTS

Item	Designation	Mass (lb_m)	
		Horizontal Coil	Vertical Coil
1	Superconducting coil and copper coil	32.5	32.5
2	304 stainless steel support tube, 3-1/2-inch SCH5	13.02	13.02
3	304 stainless steel support plate, 7 x 7 x 3/8 inch	5.33	5.33
4	Aluminum support plate	2.450	--
5	Fastening bolts for coils	2.500	2.5
6	Textolite plates and leads	3.0	3.0
7	304 stainless steel tube flange	3.43	3.43
8	304 stainless steel disk	1.26	1.26
9	Steel inner cylinder for rubber mounting	12.50	12.50
10	Steel disk for impact	9.00	9.00
11	Two aluminum support plates	--	8
12	Assembly mass m_1	85	90

LINEAR SHOCK TESTS

To determine an average value of acceleration and shock duration, the following assumptions are taken into account:

- Collision of the falling weight with all of the lead prism shock absorbers occurs simultaneously and is considered to be ideally plastic.
- Impact force is assumed to be constant during the deformation and equal to the average yield strength of the lead prisms given in Figure 17.
- Loss of kinetic energy must be equal to the work of internal stresses in the lead prism.

The average acceleration, σ, and the corresponding shock duration, δt, can be determined by the following relations (Ref. 2):

$$\alpha = \frac{A \cdot S}{m_1}$$

$$\delta t = \frac{\sqrt{2gH}\, m_2}{(m_1 + m_2)\alpha} \qquad (2)$$

where:

A = Average area of lead prisms during deformation

g = Standard gravity

H = Vertical distance weights fall before striking

m_1 = Mass of coils and support

m_2 = Mass of falling weights

δt = Shock duration

α = Average linear acceleration

S = Average yield strength of lead during deformation

The test setup for applying linear shocks is shown in Figures 1 and 3. The test procedure is:

1. The dewar is evacuated, then filled with warm helium gas to a pressure that is maintained slightly above atmospheric pressure. To cool the dewar and the coil assembly gradually, the outer jacket of the dewar is maintained at liquid nitrogen temperature for about 12 to 24 hours.
2. Liquid helium is transferred slowly into the dewar to reach a liquid level about 4 inches above the superconducting coil.
3. The coil is energized by the d-c power supply at a constant voltage of 0.2 volt until it quenches. The purpose of this test is to determine the critical current of the coil prior to the shock experiment and to ascertain that the result is consistent with previous critical current test data. (Previous tests were run without the support structure.)
4. The weights are set to a predetermined height from the top of the plate and a set of lead prisms is positioned symmetrically at the plate surface.
5. The coil is energized at a constant voltage of 0.2 volt until the current reaches a predetermined value. Then the power supply is set in a control mode, to maintain a constant current by varying the voltage across the coil.
6. The weights are released, and the acceleration during the impact is recorded on the storage oscilloscope.
7. When the series of shock tests is terminated, the coil is quenched and the critical current is measured.

The critical current of the superconducting coil was measured before and after each series of shock tests and was always found in the region $450 < I_{critical} < 460$ ($I_{critical} = 455$, as determined from critical current test data).

Table 4 and Figure 18 give the results for the series of tests in which the coil axis is vertical. The tests were repeatable and consistent, and the following conclusions can readily be derived:

- Coil performance is not impaired for currents up to 400 amperes (88 percent of the critical current) and peak accelerations up to 1700 g or average accelerations up to 260 g.
- For peak accelerations above 1800 g or average accelerations above 330 g, the superconductive coil quenches consistently at currents of 350 amperes and above.

Table 4

LINEAR SHOCK TESTS FOR COIL ASSEMBLY WITH PRINCIPAL AXIS VERTICAL

Test	Weight (lb)	Area (in^2)	Lead Prisms Height (in.) Before Shock	Lead Prisms Height (in.) After Shock	Striking Distance (in.)	Coil Current (amperes)	Average Acceleration (g)	Average Shock Duration (ms)	Peak Acceleration (g)	Coil Mode
1	23	2	0.525	0.500	40.75	400	157	0.623	--	Superconductive
2	45	2	0.525	0.4675	42.125	400	167	0.968	--	Superconductive
3	66	2	0.525	0.435	42.625	400	182	1.128	--	Superconductive
4	86	2	0.525	0.4175	42.125	400	210	1.118	--	Superconductive
5	86	3	0.525	0.4517	42.75	400	263	0.900	--	Superconductive
6	86	3	0.525	0.457	42.375	420	258	0.900	--	Normal
7	86	3	0.525	0.461	42.75	440	260	0.900	--	Normal
8	86	4	0.525	0.4705	42.375	350	330	0.713	1883	Normal
9	86	4	0.525	0.4712	42.75	400	328	0.713	1883	Normal
10	86	2	1.00	0.837	41.75	400	130	2.24	1370	Superconductive
11	86	3	1.00	0.893	41.75	400	183	1.560	1370	Superconductive
12	86	4	1.00	0.9185	41.625	400	233	1.185	1712	Superconductive

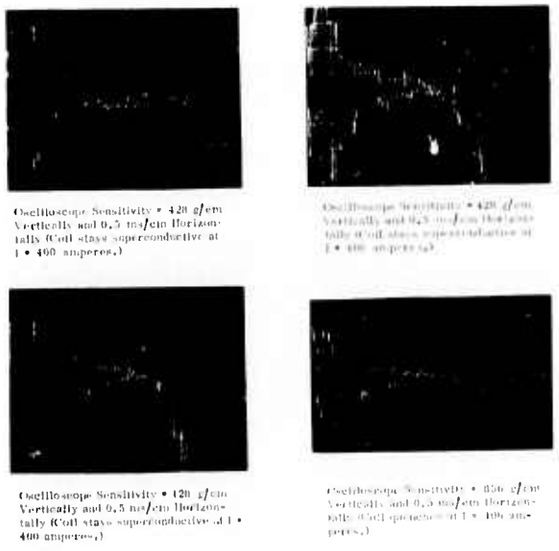

Figure 18. Linear Shock Tests for Coil Assembly with Principal Axis Vertical

The series of linear shock tests was repeated for the configuration in which the coil axis is horizontal (Figures 2 and 10). The results are given in Table 5, and Figure 19 gives the accelerometer readings as recorded by the oscilloscope. The conclusions drawn from these series of tests can be summarized:

- Coil performance is not affected for currents up to 440 amperes (97 percent of the critical current) when it is subjected to shocks of 700-g peak acceleration or 112-g average acceleration.
- The coil, energized at currents of 300 amperes and above, quenches at peak accelerations of 770 g or average accelerations of 160 g.

Table 5

LINEAR SHOCK TESTS FOR COIL ASSEMBLY WITH PRINCIPAL AXIS HORIZONTAL

Test	Weight (lb)	Area (in^2)	Lead Pristas Height (in.)		Striking Distance (in.)	Coil Current (amperes)	Average Acceleration (g)	Average Shock Duration (ms)	Peak Acceleration (g)	Coil Mode
			Before Shock	After Shock						
1	45	2	0.525	0.462	43.5	400	160	0.988	750	Normal
2	45	1	1.000	0.826	43	300	62	3.210	214	Superconductive
3	45	1	1.000	0.842	43	350	62	3.210	282	Superconductive
4	45	1	1.000	0.821	43	400	62	3.210	214	Superconductive
5	45	1	1.000	2.822	43	440	62	3.210	300	Superconductive
6	45	2	0.525	0.465	43.5	300	160	0.988	770	Normal
7	45	1.5	1.000	0.874	43	300	88	2.184	514	Superconductive
8	45	1.5	1.000	0.902	43	350	88	2.184	600	Superconductive
9	45	1.5	1.000	0.881	43	400	88	2.184	642	Superconductive
10	45	1.5	1.000	0.865	43	440	88	2.184	642	Superconductive
11	45	2.0	1.000	0.913	43	440	112	1.680	706	Superconductive
12	45	2.0	0.525	0.465	43	440	160	0.988	770	Normal

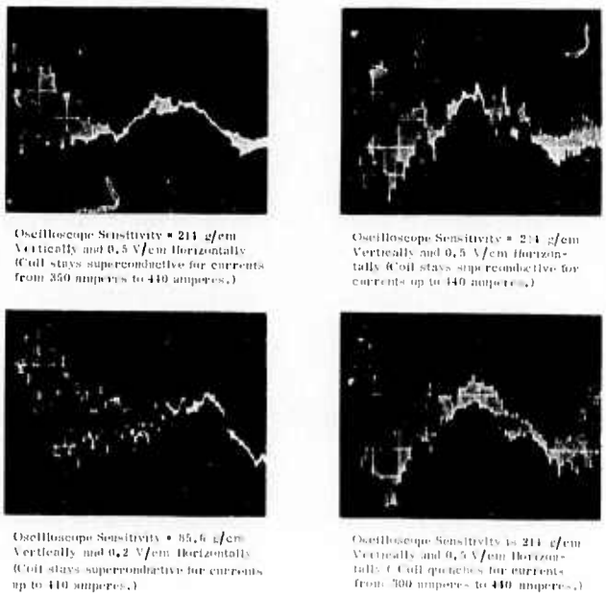

Oscilloscope Sensitivity = 214 g/cm Vertically and 0.5 V/cm Horizontally (Coil stays superconductive for currents from 350 amperes to 440 amperes.)

Oscilloscope Sensitivity = 214 g/cm Vertically and 0.5 V/cm Horizontally (Coil stays superconductive for currents up to 440 amperes.)

Oscilloscope Sensitivity = 85.6 g/cm Vertically and 0.2 V/cm Horizontally (Coil stays superconductive for currents up to 440 amperes.)

Oscilloscope Sensitivity is 214 g/cm Vertically and 0.5 V/cm Horizontally (Coil quenches for currents from 300 amperes to 440 amperes.)

Figure 19. Linear Shock Tests for Coil Assembly with Principal Axis Horizontal

The accelerometer signals that are recorded by the oscilloscope correspond to the local acceleration due to a series of longitudinal compression and tension waves that are generated successively by the series of impacts to the lead prisms and subsequent reflections at the other end of the tube support. These waves propagate through the stainless steel tube at constant velocity:

$$C_o = \sqrt{\frac{E}{\rho}} = 16090 \text{ fps} \qquad (3)$$

where:

$E = 28 \times 10^6$ = Young's modulus of 304 stainless steel (psi)

$\rho = 0.29$ = density of 304 stainless steel (lb_m/in^3)

To evaluate the significance of lower compression forces between coils and their Textolite disk supports, the assembly of coils with horizontal principal axes was tightened at room temperature using a moderate bolt torque of about 200 in.-lb_f. The coil assembly was cooled to 4.2°K (as outlined above), the superconductive coil was energized at 400 amperes, and it was subjected to a series of shock tests of average acceleration, from 60 to 260 g, and corresponding peak acceleration, from 200 to 1700 g. The coil quenched after each applied shock, verifying the postulation of local frictional heating due to the instantaneous relative motion between coils and their supports.

TORSIONAL SHOCK TESTS

The torsional impact is applied to aluminum crank B (Figure 2) by a pendulum of adjustable weight, which is released from a predetermined height. A thick walled steel pipe is rigidly mounted to the foundation (Figure 4) opposite the impact surface, to serve as a stopper. The impact is absorbed by a short lead pipe attached to the weight and a set of lead prisms that are inserted between the aluminum crank and the stopper (Figure 4).

To define an average acceleration and shock duration, the collision is assumed to result in ideally plastic deformation of the lead prisms at constant stress equal to the average yield strength of the prism. Under these assumptions, the average angular and linear acceleration at a given point of mass m_1 can be determined from the following expressions (Ref. 1):

$$\dot{W} = \frac{A \cdot S \cdot R}{I} \qquad (4)$$

$$\alpha = \dot{W} \cdot r = \frac{A \cdot S \cdot R \cdot r}{I} \qquad (5)$$

where:

α = Average linear acceleration at a given point of mass m at radius r

R = Radius at the point of impact from the axis of rotation

$\dot{W}$ = Average angular acceleration of mass m_1

A = Average area of lead prisms during deformation

m_1 = Mass of coils and support

I = Polar moment of inertia of mass m_1 about the vertical axis of rotation

The polar moment of inertia, I, for the coil assemblies of either vertical or horizontal principal axis, is summarized in Table 6.

Table 6

POLAR MOMENT OF INERTIA OF COILS AND SUPPORT

Item	Designation	Polar Moment of Inertia (lb_m-in^2)	
		Horizontal Coil	Vertical Coil
1	Superconducting coil and copper coil	195	182
2	304 stainless steel support tube, 3-1/2-inch SCH5	50	50
3	304 stainless steel support plate, 7 x 7 x 3/8 inch	43.5	43.5
4	Aluminum support plate, 7 x 7 x 1/2 inch	20.0	--
5	Fastening bolts for coils	37.8	19
6	Textolite plates and leads	40.0	60
7	304 stainless steel tube flange	22.2	22.2
8	304 stainless steel disk	2.3	2.3
9	Steel inner cylinder for rubber mounting	26.6	26.6
10	Steel disk for impact	55.1	55.1
11	Two aluminum support plates, 7 x 9 x 1/2 inch	--	110
12	Aluminum bar, 2-1/2 x 2-1/2 x 7 inches	71.5	71.5
13	Steel impact disk for aluminum bar	28.5	28.5
14	Total polar moment of inertia, I	592.5	670.7

COIL ASSEMBLY WITH AXIS VERTICAL

The accelerometer was mounted on top of the aluminum crank (Figure 4) at a 6-inch radial distance from the axis of rotation. Thus the linear acceleration at the coil outer diameter (6 inches) is half the measured acceleration. Table 7 and Figure 20 summarize the data for the torsional shock test for the

Table 7

TORSIONAL SHOCK TEST FOR COIL ASSEMBLY WITH VERTICAL AXIS

Test	Weight (lb)	Area (in^2)	Lead Prisms Height (in.)		Striking Distance (in.)	Coil Current (amperes)	Calculated Average Acceleration, Coil OD (g)	Average Acceleration at Coil OD from Oscilloscope (g)	Shock Duration (ms)	Coil Mode
			Before Shock	After Shock						
1	26	0.5	--	--	60	425	--	850 550 360 250 170	0.0 0.5 1.0 1.0 2.0	Superconductive
2	26	1.0	--	--	60	440	--	750 470	1.0 3.0	Superconductive
3	26	0.525	0.525	0.3055	60	420	--	680 425 280 130	0.0 0.7 1.1 0.9	Superconductive
4	26	1	0.525	0.400	60	420	250	1700 342 171	0.0 1.0 0.7	Superconductive
5	26	1	0.525	0.395	60	440	250	1370 342 171	0.0 1.0 0.7	Superconductive
6	30	1	0.525	0.405	60	440	250	1700 428 214	0.0 1.0 0.7	Superconductive
7	48.5	--	--	--	60	440	--	214	1.5	Superconductive

Test 1 -- Oscilloscope Sensitivity = 428 g/cm Vertically and 0.5 ms/cm Horizontally (SC was energized at 425 amperes and it remained superconductive after the shock.)

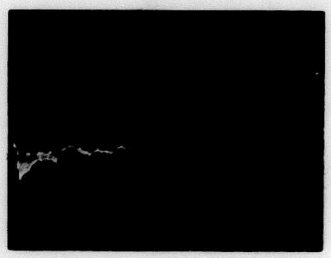

Test 3 -- Oscilloscope Sensitivity = 856 g/cm Vertically and 0.5 ms/cm Horizontally (SC is energized at 420 amperes and it remained superconductive after the shock.)

Test 2 -- Oscilloscope Sensitivity = 428 g/cm Vertically and 0.5 ms/cm Horizontally (SC was energized at 440 amperes and it remained superconductive after the shock.)

Test 6 -- Oscilloscope Sensitivity is 856 g/cm Vertically and 0.5 ms/cm Horizontally (SC was energized at 440 amperes and it remained super conductive after the shock.)

Figure 20. Accelerometer Output at 6-Inch Radius for Torsional Shock Tests of Superconducting Coil Assembled with Axis Vertical

coil assembly with a vertical axis. As anticipated, the oscilloscope readings indicate an initially high acceleration, lasting about 0.2 to 0.3 ms, followed by a diminishing deceleration due to the deformation of the lead prisms.

The results of these tests indicate that the performance of the superconducting coil is not impaired for currents up to 97 percent of the critical current and linear accelerations at the coil outer diameter of peak absolute value up to 1700 g and average value up to 470 g for 3 ms.

COIL ASSEMBLY WITH AXIS HORIZONTAL

The tests were repeated for the case in which the coil axis is horizontal, and the acceleration was measured at a 6-inch radial distance. The test data are presented in Table 8, and Figure 21 displays the accelerometer readings.

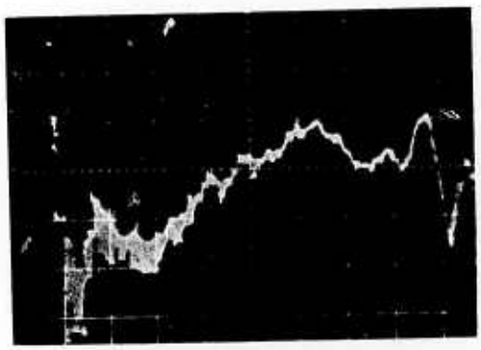

Test 1 -- Oscilloscope Sensitivity = 214 g/cm Vertically and 0.5 ms/cm Horizontally (SC is energized at 300 amperes and remains superconducting after the shock.)

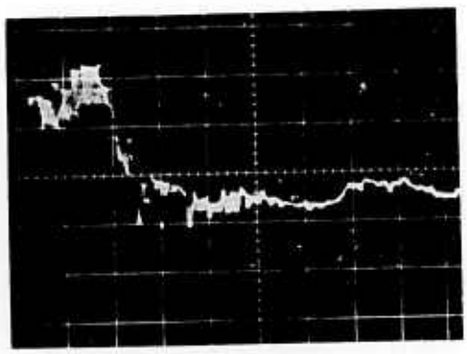

Test 3 -- Oscilloscope Sensitivity = 856 g/cm Vertically and 0.2 ms/cm Horizontally (SC is energized at 440 amperes and remains superconductive following the shock.)

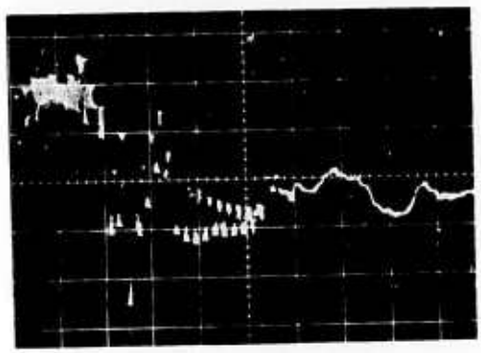

Test 4 -- Oscilloscope Sensitivity = 856 g/cm Vertically and 0.2 ms/cm Horizontally (SC is energized at 440 amperes and stays superconductive following the shock.)

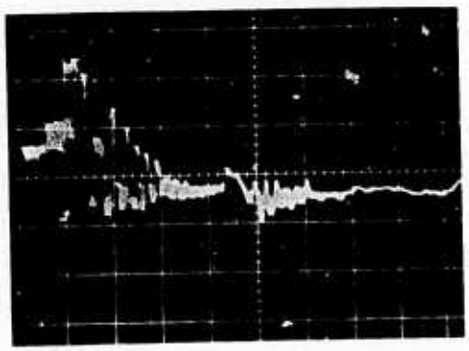

Test 5 -- Oscilloscope Sensitivity = 2140 g/cm Vertically and 0.2 ms/cm Horizontally (SC is energized at 445 amperes and stays superconductive after the shock.)

Figure 21. Accelerometer Output at 6-Inch Radius for Torsional Tests of Superconducting Coil Assembled with Axis Horizontal

Table 8

TORSIONAL SHOCK TEST FOR COIL ASSEMBLY WITH HORIZONTAL AXIS

Test	Weight (lb)	Area (in²)	Lead Prisms Height (in.) Before Shock	Lead Prisms Height (in.) After Shock	Striking Distance (in.)	Coil Current (amperes)	Calculated Average Acceleration, Coil OD (g)	Average Acceleration at Coil OD from Oscilloscope (g)	Shock Duration (ms)	Coil Mode
1	26	1	0.525	0.425	60	300	210	375 214 100	0.2 0.8 0.6	Superconductive
2	26	1	0.525	0.425	60	400	210	278 150	1.1 0.8	Superconductive
3	26	1	0.525	0.415	60	440	210	856 300 171	0.4 0.7 0.6	Superconductive
4	48.5	1	0.525	0.340	60	440	250	856 513 214	0.4 0.6 0.5	Superconductive
5	48.5	2	0.525	0.420	60	445	420	2570 530	0 1.5	Superconductive

It is evident from these tests that the coil performance was not affected for critical currents up to 445 amperes and linear accelerations at the coil outer diameter of peak value up to 2570 g and average value up to 530 g for 1.5 ms. Although it is desirable to determine the peak acceleration for which the coil quenches, the test apparatus was not designed to induce higher accelerations, in view of the fact that such accelerations are not to be anticipated in superconductive propulsion systems for Navy applications.

LINEAR VIBRATION TESTS

The vibrator exciter is mounted on the dewar cover plate, as shown in Figure 5. The vibrations are excited by a spherical roller bearing with an eccentric adapter sleeve of 0.030-inch eccentricity. The amplitude of the vibration is determined by the eccentricity of the adapter sleeve, while the frequency of the vibration can vary by varying the speed of the motor.

The vibratory force is exerted parallel to the vertical principal axis of the assembly; however, small misalignment relative to the true centerline axis is inherently inevitable and results in higher amplitude vibration at the outer diameter of the top plate relative to the one excited near the center. Therefore, the resulting vibration at the coil outer diameter (assembly with vertical coil axis) will yield a higher acceleration at that location relative to the one at the center. To determine the acceleration at the coil outer diameter, the accelerometer is mounted on the top plate at a 3-inch radius.

The series of vibration tests was carried out as follows:

1. The superconducting coil was energized at a constant voltage of 0.2 volt until it quenched. The critical current obtained was compared to previous experimental data.
2. The superconducting coil was energized and maintained at a constant current.

3. The vibrator exciter was turned on and the motor speed was varied incrementally and measured using a strobe light.

4. The accelerometer output voltage was measured on a Ballantine true rms voltmeter (model 323-01), and the voltage was recorded by the storage oscilloscope.

5. Upon completion of the series of tests, the coil was quenched to determine the critical current.

The test results for the assembly of coils with the axis vertical is given in Table 9, and Figure 22 shows the accelerometer output as recorded by the oscilloscope.

Table 9

LINEAR VIBRATION TESTS FOR COIL ASSEMBLY WITH PRINCIPAL AXIS VERTICAL

Test	Motor Speed (rpm)	Time Duration (seconds)	Coil Current (amperes)	Accelerometer Output (volts rms)	Acceleration, Coil OD (g)	Acceleration, Coil Center (g)	Coil Mode
1	--	--	442	--	--	--	Normal
2	1000	15	400	0.122	3.7	0.85	Superconductive
3	1200	15	400	0.180	5.45	1.22	Superconductive
4	1390	15	400	0.260	7.88	1.65	Superconductive
5	1600	15	400	0.335	10.02	2.18	Superconductive
6	1820	15	400	0.550	16.62	2.82	Superconductive
7	2200	15	400	0.640	19.39	4.12	Superconductive
8	2920	15	400	0.950	28.78	7.26	Superconductive
9	900	15	420	0.165	5.0	0.69	Superconductive
10	1140	15	420	0.240	7.27	1.10	Superconductive
11	1400	15	420	0.300	9.09	1.67	Superconductive
12	1640	15	420	0.340	10.30	2.29	Superconductive
13	1860	15	420	0.470	14.24	2.95	Superconductive
14	2180	15	420	0.580	17.57	4.05	Superconductive
15	2940	15	420	0.780	23.63	7.36	Superconductive
16	1620	15	440	0.300	9.09	2.23	Superconductive
17	3000	15	440	0.960	29.09	7.66	Superconductive
18	--	--	452	--	--	--	Normal

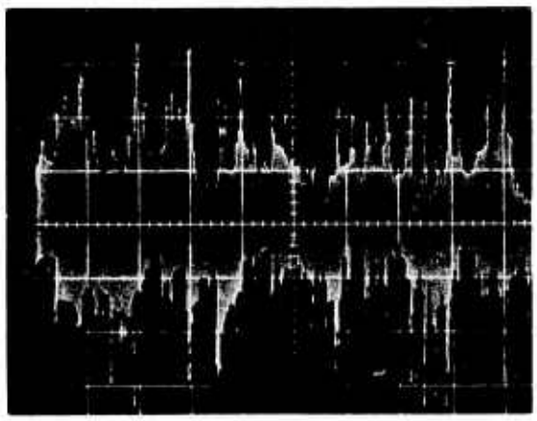

Figure 22. Accelerometer Output at 6-Inch Diameter for Linear Vibration Tests with Coil Principal Axis Vertical (Oscilloscope sensitivity is 21.4 g/cm vertically and 10 ms/cm horizontally.)

The noise associated with the accelerometer output is partly due to the misalignment of the exciting vibratory force relative to the true centerline axis and is partly due to the unequal reaction force of the three Belleville springs that are mounted under the top circular plate. These springs are spaced 120 degrees apart on a centerline circle 6 inches in diameter. Nevertheless, the voltmeter reading provides a more accurate means for determining the peak acceleration.

The conclusions drawn from these tests can be summarized. The superconducting coil performance is not affected at currents up to 440 amperes when subjected to linear vibration of variable frequency from 1000 to 3000 rpm, double amplitude of 0.060 inch, and peak accelerations up to 30 g. Further, the linear vibration tests were carried out for the assembly of coils with a horizontal principal axis, and the test data are presented in Table 10. Figure 23 gives the accelerometer output as recorded by the oscilloscope at 3300-rpm vibration frequency. The test results indicate that the superconducting coil mounted with its axis horizontal and energized at currents up to 451 amperes can sustain linear vibrations of frequency from 920 to 3300 rpm and peak accelerations up to 40 g.

TORSIONAL VIBRATION TESTS

The torsional vibrations are excited by applying linear vibrations at the aluminum crank at a 7-inch radial distance. The vibration force is exerted at the rolling contact of the bearing outer diameter, and it is reacted by the force of three Belleville springs at the opposite side of the aluminum crank (Figure 6).

Consequently, the force is not fixed in position and the resulting vibration is not purely torsional or free of noise. As before, the accelerometer is mounted on the crank at a 6-inch radius. The series of tests was performed in sequence similar to the one that was followed in the linear vibration experiments.

COIL ASSEMBLY WITH AXIS VERTICAL

The test data are summarized in Table 11, and Figure 24 gives the accelerometer output voltage at a 3820-rpm vibrator frequency. The results demonstrate that the coil performance is not impaired at currents up to 445 amperes for torsional vibration frequencies from 500 to 3840 rpm, double amplitude of 0.00857 radian, and linear accelerations up to 13.5 g at the coil outer diameter.

COIL ASSEMBLY WITH AXIS HORIZONTAL

As before, the torsional tests were carried out by varying the frequency of the vibrator and keeping the amplitude and the coil current constant. The test data are presented in Table 12, and the accelerometer output is shown in Figure 25.

Table 10

LINEAR VIBRATION TEST FOR COIL ASSEMBLY
WITH PRINCIPAL AXIS HORIZONTAL

Test	Motor Speed (rpm)	Time Duration (seconds)	Coil Current (amperes)	Accelerometer Output (volts rms)	Acceleration, Coil OD (g)	Acceleration Coil Center (g)	Coil Mode
1	--	--	460	--	--	--	Normal
2	920	20	400	0.110	3.33	0.72	Superconductive
3	1600	20	400	0.280	8.48	2.18	Superconductive
4	2300	20	400	0.550	10.67	4.50	Superconductive
5	3000	20	400	1.00	30.30	7.66	Superconductive
6	3300	20	400	1.20	36.36	9.27	Superconductive
7	920	20	440	0.150	4.55	0.72	Superconductive
8	1600	20	440	0.360	10.90	2.18	Superconductive
9	2300	20	440	0.660	20.00	4.50	Superconductive
10	3000	20	440	1.200	36.36	7.66	Superconductive
11	3300	20	440	1.300	40.00	9.77	Superconductive
12	920	20	451	0.170	5.15	0.72	Superconductive
13	1600	20	451	0.380	11.51	2.18	Superconductive
14	2300	20	451	0.670	20.30	4.50	Superconductive
15	3000	20	451	1.00	30.30	7.66	Superconductive
16	3300	20	451	1.20	36.36	9.27	Superconductive
17	--	--	455	--	--	--	Normal

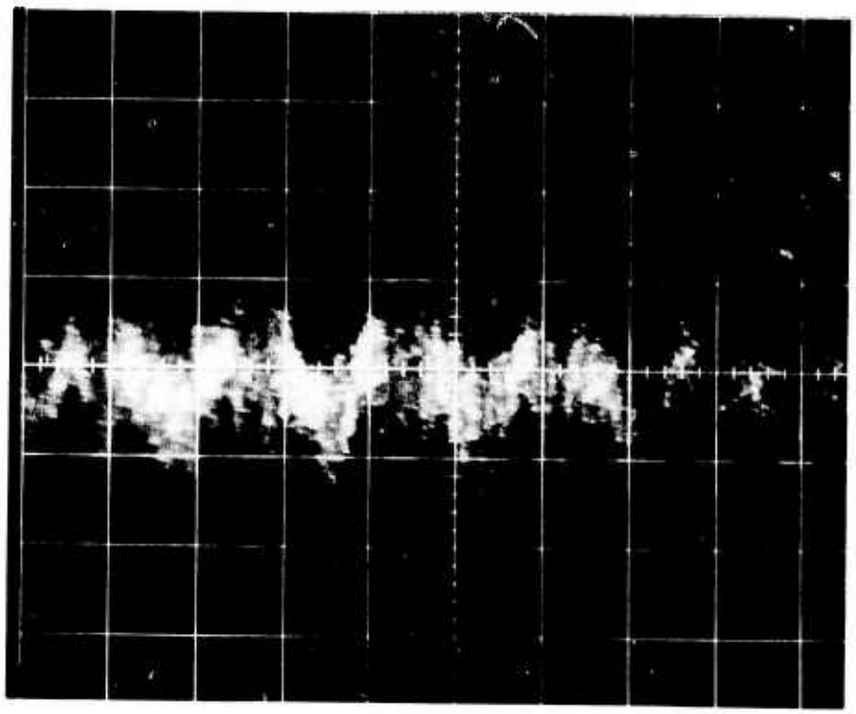

Figure 23. Accelerometer Output at 6-Inch Diameter for Linear Vibration Tests with Coil Axis Horizontal (Oscilloscope sensitivity is 42.8 g/cm vertically and 10 ms/cm horizontally.)

Table 11

TORSIONAL VIBRATION TESTS FOR COIL ASSEMBLY WITH AXIS VERTICAL

Test	Motor Speed (rpm)	Time Duration (seconds)	Coil Current (amperes)	Accelerometer Output (volts rms)	Acceleration, Coil OD (g)	Coil Mode
1	--	--	451	--	--	Normal
2	500	20	400	0.020	0.31	Superconductive
3	1040	20	400	0.062	0.94	Superconductive
4	1680	20	400	0.140	2.12	Superconductive
5	2720	20	400	0.350	5.30	Superconductive
6	3430	20	400	0.670	10.15	Superconductive
7	3800	20	400	0.800	12.1	Superconductive
8	500	20	440	0.33	0.50	Superconductive
9	1160	20	440	0.080	1.21	Superconductive
10	1840	20	440	0.158	2.40	Superconductive
11	2680	20	440	0.350	5.30	Superconductive
12	3520	20	440	0.72	10.91	Superconductive
13	3820	20	440	0.90	13.63	Superconductive
14	500	20	448	0.045	0.68	Superconductive
15	1180	20	445	0.090	1.36	Superconductive
16	1800	20	444	0.200	3.03	Superconductive
17	2600	20	445	0.520	7.88	Superconductive
18	3500	20	444	0.740	11.21	Superconductive
19	3840	20	445	0.800	12.12	Superconductive
20	--	--	458	--	--	Normal

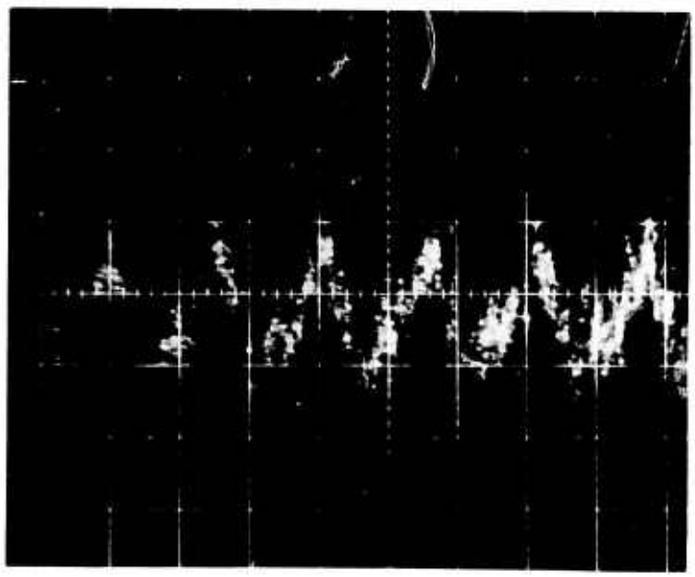

Figure 24. Accelerometer Output at 6-Inch Radius for Torsional Vibration Tests of Coils with Axis Vertical (Oscilloscope sensitivity is 21.4 g/cm vertically and 10 ms/cm horizontally.)

Table 12

TORSIONAL VIBRATION TESTS FOR COIL ASSEMBLY WITH AXIS HORIZONTAL

Test	Motor Speed (rpm)	Time Duration (seconds)	Coil Current (amperes)	Accelerometer Output (volts rms)	Acceleration, Coil OD (g)	Coil Mode
1	--	--	451	--	--	Normal
2	500	20	400	0.036	0.55	Superconductive
3	1120	20	400	0.140	2.12	Superconductive
4	1820	20	400	0.200	3.03	Superconductive
5	2620	20	400	0.420	6.36	Superconductive
6	3400	20	400	0.610	9.24	Superconductive
7	3800	20	400	0.780	11.82	Superconductive
8	500	20	440	0.033	0.50	Superconductive
9	1200	20	440	0.145	2.20	Superconductive
10	1820	20	440	0.240	3.64	Superconductive
11	2600	20	440	0.420	6.36	Superconductive
12	3380	20	440	0.620	9.39	Superconductive
13	3760	20	440	0.750	11.36	Superconductive
14	500	20	447	0.032	0.48	Superconductive
15	1140	20	445	0.135	2.05	Superconductive
16	1800	20	444	0.280	4.24	Superconductive
17	7680	20	445	0.580	8.79	Superconductive
18	3400	20	445	0.720	10.91	Superconductive
19	3800	20	445	0.880	13.33	Superconductive
20	--	--	461	--	--	Normal

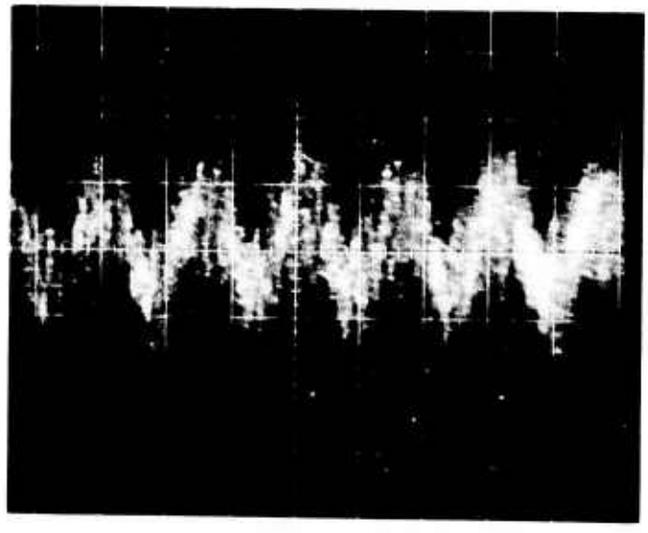

Figure 25. Accelerometer Output at 6-Inch Radius for Torsional Vibration Tests of Coils with Axis Horizontal (Oscilloscope sensitivity is 21.4 g/cm vertically and 10 ms/cm horizontally.)

As anticipated, the coil remained superconductive at currents up to 445 amperes, vibrator frequencies from 500 to 3800 rpm, double amplitude of 0.00857 radian, and linear accelerations at a 6-inch diameter -- up to 13 g.

COIL COMPOSITE COMPRESSIVE STRENGTH TESTS

The compressive yield strength and Young's modulus of epoxy impregnated composite windings of superconductor wire are of considerable interest with regard to the structural support of the coil. Room temperature data of the compressive yield strength are not sufficient to predict the yield strength at 4.2°K. Further, the compressive stresses of firmly supported coils, below the elastic limit at room temperature, could increase considerably when the structure is cooled to 4.2°K, due to differential contraction of the winding-structural assembly. In some cases, the compressive stresses could exceed the yield strength of the coil composite at 4.2°K. Consequently permanent deformation can occur, which may loosen the winding-structural assembly when thermal cycling occurs from room temperature to 4.2°K.

The modulus of elasticity as well as the compressive yield strength of the coil composite will be investigated experimentally at room temperature and 4.2°K for directions perpendicular to the wire and parallel or perpendicular to the glass roving. Because the properties of the glass cloth epoxy impregnated windings in directions perpendicular to the wire are expected to be nearly independent of the wire material properties, the specimens were cut from coils wound with round copper wires of the same diameter as the superconductor wire.

TEST APPARATUS

The test apparatus displayed in Figure 26 consists of Enerpac hydraulic cylinder C, of 100,000-pound capacity; concentric stainless steel tubes A and B; and specimen support plate S, which is rigidly fastened to tube B through flange F and bolts D.

Outer tube B is fastened to the jacket of the hydraulic cylinder, and it is further supported from the dewar cover plate, as shown in Figure 26. The lower end of tube B is welded to flange F, which then provides support to the test specimen through bolts D and plate S.

Inner tube A is free to slide within outer tube B and transmits the compressive force of the cylinder piston to the test specimen. The test specimens are cut from a cylindrical coil of 6.20-inch outer diameter, 3-inch bore diameter, and 2.5-inch length. The coil is wound with copper wire 0.050 inch in diameter.

To evaluate the coil properties in the radial direction, perpendicular to the wire and the glass roving, specimens in the shape of annular sectors are

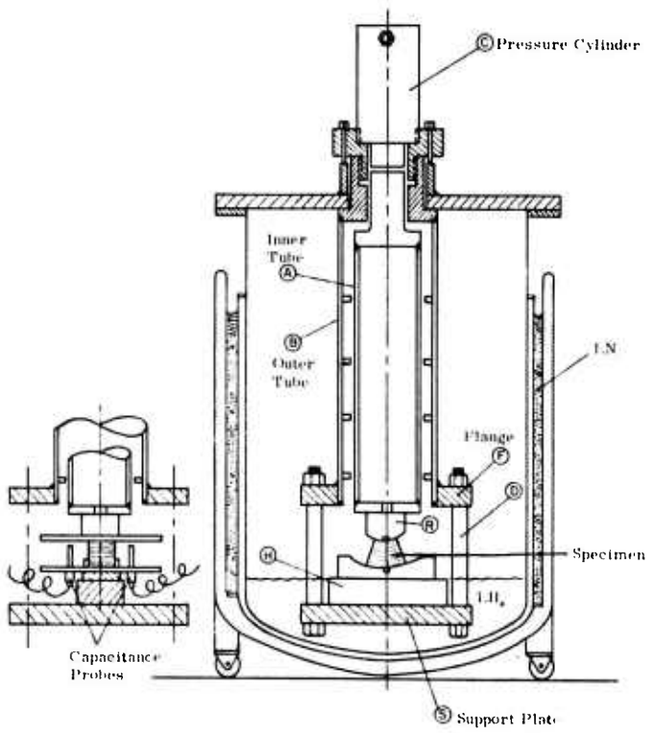

Figure 26. Test Apparatus Setup for Radial Compression Tests of Core Composite Specimens

cut from the coil and placed on a prismatic housing, H, with their outer cylindrical surface resting against the housing (Figure 27). The force is exerted to the inner cylindrical surface of the specimen by pushing rod R, which is attached to tube A.

The properties of the coil in the axial direction, perpendicular to the wire and parallel to the glass roving, are determined by compressing the specimens axially between two parallel plane surfaces, as shown in Figure 28. As before, the specimens are cut from the coil in the shape of annular sectors.

Figure 29 gives an overall view of the test apparatus and instrumentation.

TEST RESULTS

The compressive yield strength and modulus of elasticity of epoxy impregnated composite windings was investigated experimentally at room temperature and liquid helium temperature. The results, summarized in Table 13, indicate that the yield strength and Young's modulus of the composite at liquid helium temperature increase by about 40 to 80 percent relative to their values at room temperature. Further, the yield strength of the composite perpendicular to the glass roving is higher relative to the composite parallel to the glass roving.

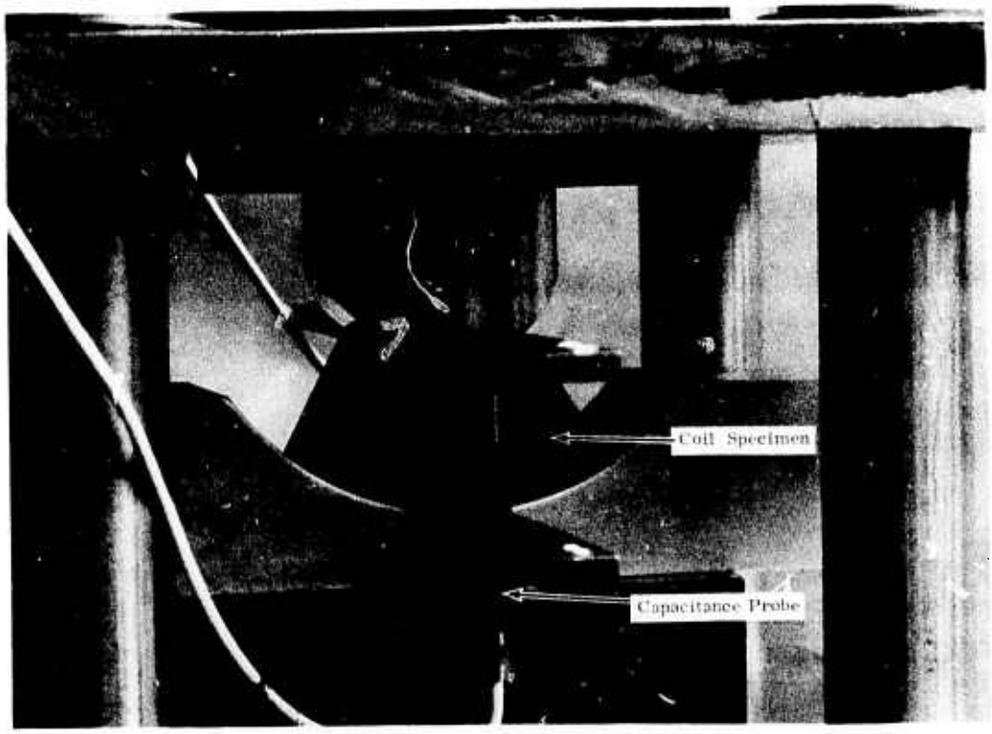

Figure 27. Coil Composite Specimen Setup for Radial Compression Tests

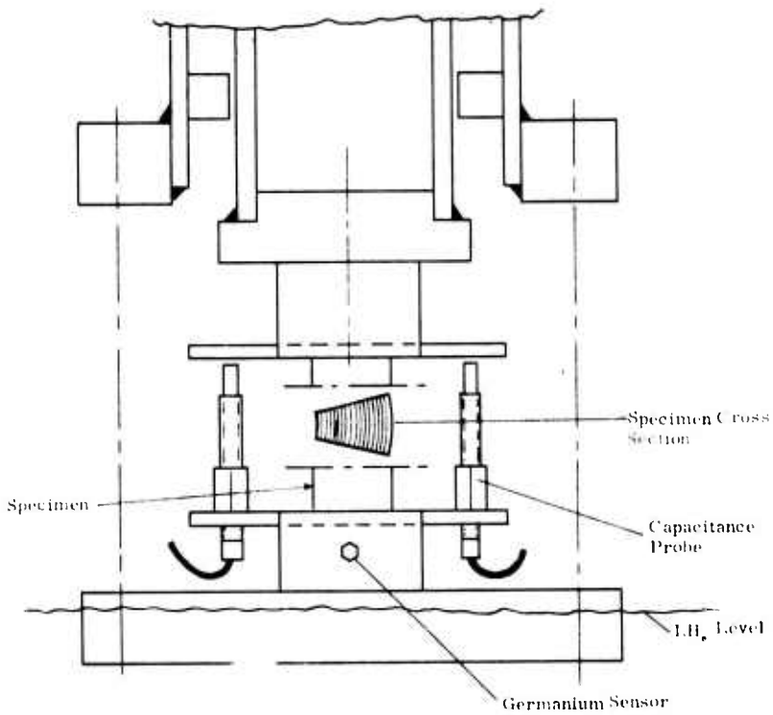

Figure 28. Arrangement for Testing Coil Composite Specimens in Axial Compression

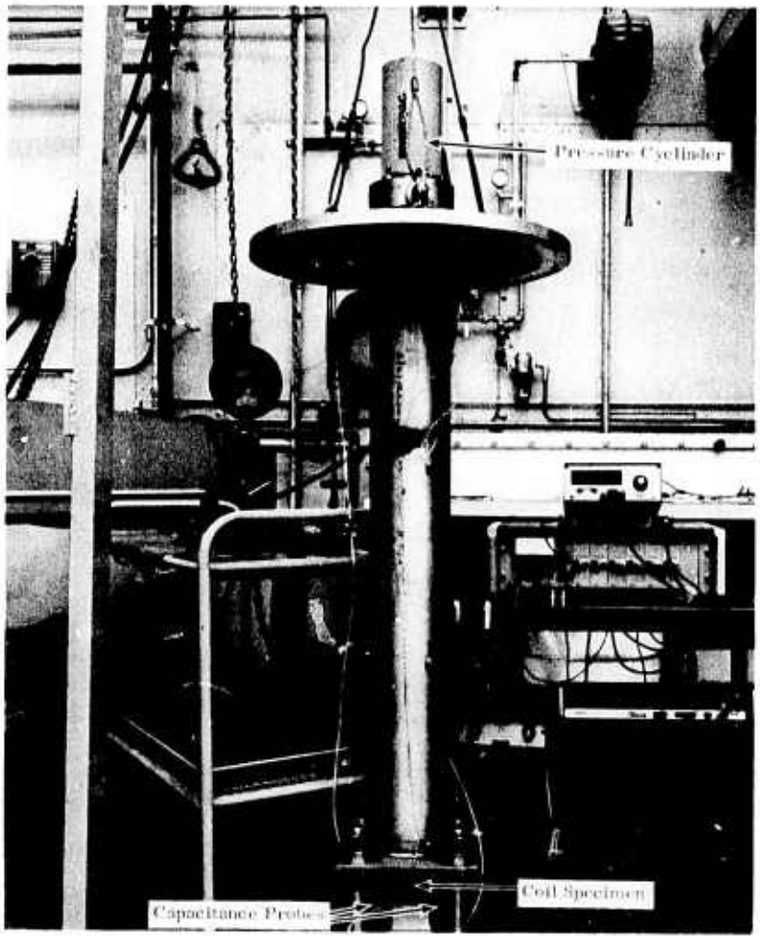

Figure 29. Test Apparatus and Instrumentation for Coil Composite Strength Experiments

Table 13

COMPRESSIVE YIELD STRENGTH AND MODULUS OF ELASTICITY OF COMPOSITE WINDINGS AT ROOM TEMPERATURE AND LIQUID HELIUM TEMPERATURE

Direction of Compression	Temperature (°K)	0.1 percent Yield Strength (psi)	Modulus of Elasticity (psi)
Normal to wire and glass roving	300	21000	2.27×10^6
Normal to wire, parallel to glass roving	300	19000	2.9×10^6
Normal to wire and glass roving	4.3	36500	3.13×10^6
Normal to wire, parallel to glass roving	4.4	27000	5.4×10^6

The yield strength and modules of elasticity of the winding composite at room temperature compare well with typical data for epoxy glass cloth Textolite composites (σ = 25,000 psi, E = 3.4 x 10^6). Consequently the mechanical properties of the winding composite are nearly independent of the properties of the conductor wire.

INSTRUMENTATION

The hydraulic pressure is applied to the Enerpac cylinder by an Enerpac hand pump (model 11-440). Hydraulic gages from 0 to 5000 psi or 0 to 16,000 psi are used to measure the pressure and determine the force applied to the test specimen. The deflection of the test specimen is measured by two capacitance probe sensors, which are mounted symmetrically about the centerline axis of inner tube A, as shown in Figures 26 and 27.

The capacitance probes were calibrated in a micrometer fixture, and their output voltage is correlated to the displacement readings of the micrometer, as shown in Figure 30. The calibration curve indicates that the sensor output is linear up to 0.014-inch displacements and that its sensitivity is:

$$E_c = 105 \text{ V/in.} \qquad (6)$$

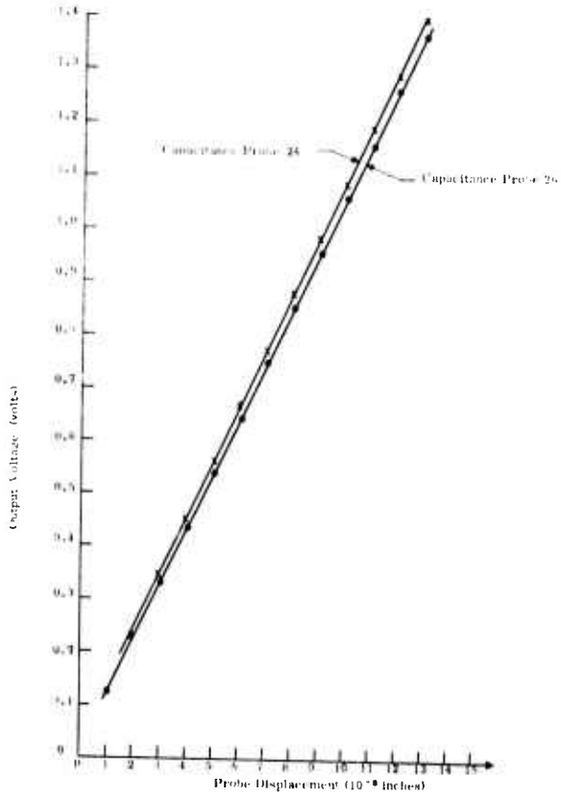

Figure 30. Calibration of Capacitance Probe Sensors in Micrometer Fixture

The calibration of the capacitance probes was carried out in air; nevertheless, it was repeated in helium gas for a few points, and the resulting deviation was less than 1 percent.

Because the capacitance probes are symmetric about the centerline axis, the displacement at the centerline corresponds to the average value of the probe readings. To measure the temperature of the test specimen, a calibrated germanium resistance cryogenic thermometer was mounted on the prism supporting the specimen. The germanium sensor (model N1J, serial 10506), manufactured by Scientific Instruments, Inc., was calibrated by the factory in the range from 4° to 40°K.

COMPRESSIVE STRENGTH TESTS

A series of radial compression tests of the coil specimens assembled on the test apparatus (Figure 27) was carried out at room temperature (300°K); Figure 31 gives the stress at the inner cylindrical surface of the specimen versus the radial contraction. The 0.1-percent yield strength of the composite at room temperature was found:

$$\sigma_{300} = 21,000 \text{ psi} \tag{7}$$

To determine Young's modulus E, let ϵ be the strain at radius r; it then follows that the radial contraction:

$$\Delta R = \int_{R_1}^{R_2} \epsilon \, dr \tag{8}$$

where R_1, R_2 are the coil inner and outer radii, respectively. From Hooke's law, the strain:

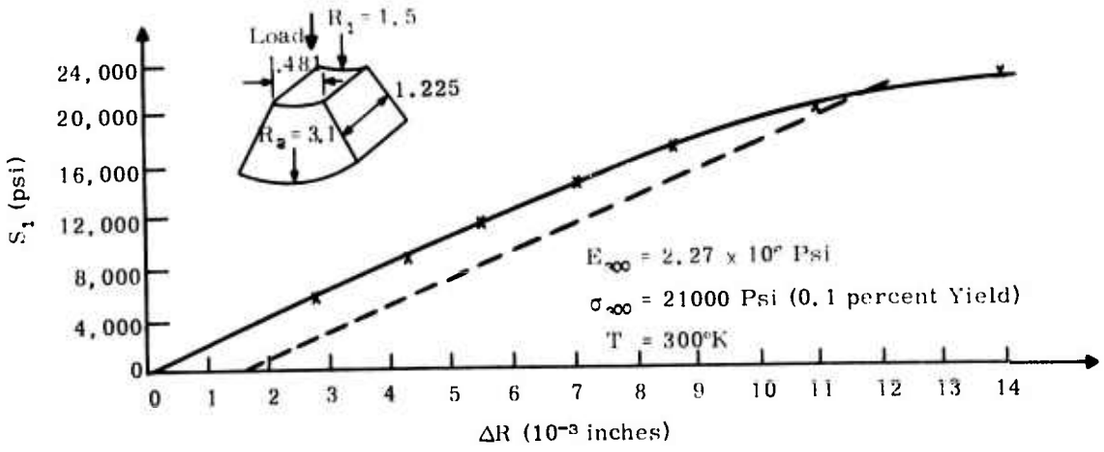

Figure 31. Bore Stress Versus Contraction for Radially Compressed Coil Specimens at Room Temperature (300°K)

$$\varepsilon = \frac{S}{E} = \frac{W}{\varphi\, rb\, E} \tag{9}$$

where:

E = Young's modulus (psi)

φ = Angle of sector (rad)

r = Radius (inches)

b = Specimen width (inches)

W = Applied load (lb_f)

Substituting in Equation 8 for ε the expression from Equation 9, the following expression results upon integration:

$$E = \frac{W}{\Delta R\, \varphi b} \quad \ln \frac{(R_2)}{R_1} \tag{10}$$

The modulus of elasticity at room temperature is then:

$$E_{300} = 2.27 \times 10^6 \text{ psi} \tag{11}$$

To perform the radial compressive tests at cryogenic temperatures, the apparatus was mounted into the dewar, and it was cooled gradually by keeping the jacket of the dewar at liquid nitrogen temperature for about 12 hours. The dewar was then filled with liquid helium, and the liquid level was maintained below the capacitance probe sensors.

The stress-deflection curve obtained at 4.3°K is shown in Figure 32, and the 0.1-percent yeild strength of the composite is:

$$\sigma_{4.3} = 36,500 \text{ psi} \tag{12}$$

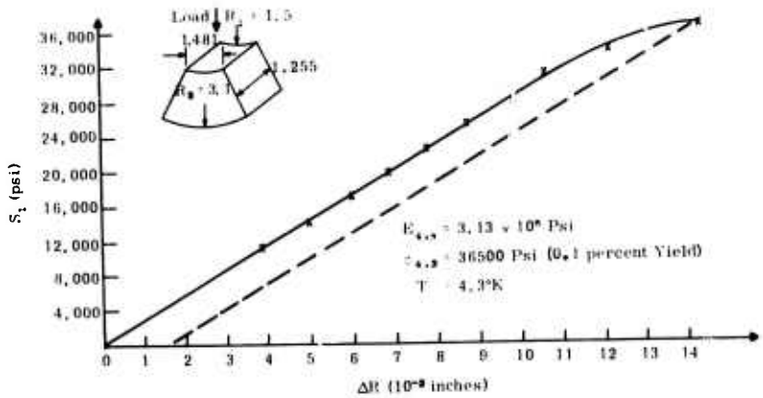

Figure 32. Bore Stress Versus Contraction for Radially Compressed Coil Specimens at 4.3°K

The modulus of elasticity at 4.3° K is determined from Equation 10; therefore:

$$E_{4.3} = 3.13 \times 10^6 \text{ psi} \tag{13}$$

To carry out the axial compression tests, the specimens are assembled in the apparatus as shown in Figure 28. The room temperature test data are plotted in Figure 33 and result in a compressive, 0.1 percent yield strength:

$$\sigma_{300} = 19,000 \text{ psi} \tag{14}$$

with a corresponding modulus of elasticity:

$$E_{300} = 2.9 \times 10^6 \text{ psi} \tag{15}$$

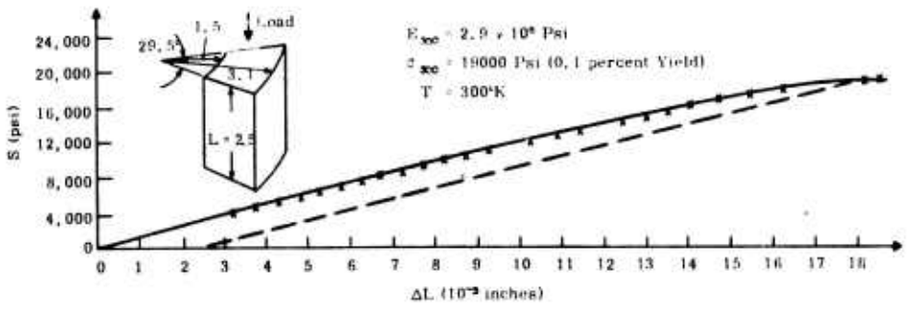

Figure 33. Stress Versus Contraction for Axially Compressed Coil Specimens at 300° K

The [illegible]s of axial compression tests was repeated at 4.4° K, and the test data are plotted in Figure 34. The resulting modulus of elasticity and 0.1 percent compressive yield strength are:

$$E_{4.4} = 5.4 \times 10^6 \text{ psi} \tag{16}$$

$$\sigma_{4.4} = 27,000 \text{ psi} \tag{17}$$

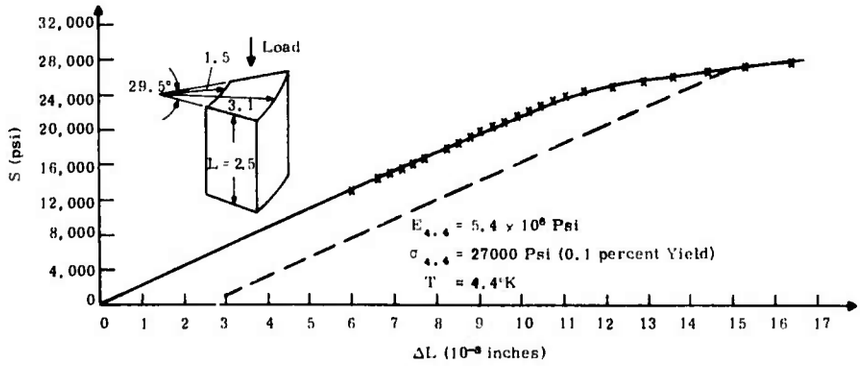

Figure 34. Stress Versus Contraction for Axially Compressed Coil Specimens at 4.4° K

Section 3

LIQUID METAL CURRENT COLLECTOR TECHNOLOGY

GENERAL DESIGN

The main purpose of this task was to design, construct, and test an unflooded current collection system using gallium as the liquid metal. Most of the previous work completed on acyclic current collection systems involved the use of NaK, which has the advantages of excellent compatibility with copper, low viscosity and density, and good electrical conductivity. The outstanding disadvantage of NaK is its highly reactive nature when in contact with oxygen, water, and many other common substances, including fluoropolymers.

Gallium, on the other hand, is a low-hazard material, being nontoxic and substantially nonreactive to oxygen and water, due to the formation of an exceedingly stable oxide film similar to the protective oxide that forms on aluminum. The main potential hazard of gallium would appear to be its tendency to amalgamate with certain metals (such as copper and copper alloys), causing an intergranular solution and eventual failure. In this respect gallium is similar to mercury; both metals are incompatible with copper alloys. Table 14 lists several pertinent properties of NaK and gallium.

Table 14

PHYSICAL PROPERTIES OF NaK-78 AND GALLIUM

Material	Composition	Specific Gravity	Electrical Conductivity (mho/m)	Viscosity (kg/m sec)	Melting Point (°C/°F)	Boiling Point (°C)
NaK-78	22 percent Na 78 percent K	0.85	2.2×10^6	4.7×10^{-4}	-11.1/12	<1000
Gallium	--	6.0	3.6×10^6	15×10^{-4}	29.8/85.6	>2000

The main shortcomings of gallium, as evidenced from inspection of Table 14, are the higher viscosity and density compared to NaK. These properties do lead to higher fluid friction losses for gallium in high-speed, fully flooded collectors, but for unflooded, low-speed systems such as would be found in propulsion system motors, the application of the loss equations developed in Reference 1 show that a gallium system can have lower losses than NaK systems (Appendix I, "Current Collector Gap Losses"). The gallium solidification temperature of 86.5° F is a nuisance factor during startup and can lead to the cracking of glass containers, but it is not an insurmountable problem.

The main objection to the use of gallium in the past can be summarized by quoting from page 21 of Reference 1:

Some of the properties of gallium and its alloys would be desirable in current-collector applications, but, unfortunately, gallium displays an unusual property that eliminates this fluid from further consideration. It has been shown that if gallium is used in sliding electrical contacts, it rapidly undergoes a physical transformation and is converted to a powder-like substance.

More recent work has shown that this powder transformation is merely due to the formation of microscopic globules of gallium having oxide skins of high mechanical stability and that their formation can be prevented or at least greatly delayed by blanketing the liquid metal with a dry, oxygen-free cover gas. Developmental systems have been successfully operated for hundreds of hours at surface speeds exceeding 5000 ft/min. Other unknowns in the operation of a gallium unflooded collector system are those that also are present in any liquid metal system (i. e., formation of spray and dust, creepage, wetting, and the liquid dynamics of free surface collectors at varying speeds). These unknowns are related to the details of specific collector configurations.

To obtain an insight into all of the above problems, a current collector test rig was designed and built to simulate the conditions actually existing in a disk acyclic machine utilizing the high magnetic flux densities of a superconducting solenoid. The test apparatus consists of a single disk generator driven by a variable speed, 25-hp, a-c motor. The generator housing has an overall diameter of 8 inches and is inserted in the bore of the dewar of a liquid helium cooled superconducting solenoid wound from a composite conductor of niobium-tin tape. The solenoid produces a magnetic flux density of approximately 6 tesla at an excitation current of 500 amperes (see Reference 3 for a description of the coil).

A cross section of the test rig is shown in Figure 35, and photographs of the test installation are shown in Figures 36 and 37. The generator and drive assembly are mounted on an aluminum bed plate 4 inches thick. A hinge mounting at the solenoid end of the plate allows the whole assembly to be canted at an angle up to 30 degrees from the horizontal, to simulate mounting and pitch angle in a ship. The drive train is best seen in Figure 37, which shows (from right to left) the 25-hp drive motor, the belt drive under its belt guard, the drive shaft with a strain gage torquemeter mounted between two flexible couplings, the generator bearing pedestal from which the generator is overhung into the dewar bore, and (on the left) the dewar of the superconducting solenoid.

The end view (Figure 36) shows the water cooled load resistor, 10,000-ampere shunt, and the bus bars leading into the test rig from the right. The metal tubing issuing from the dewar bore toward the left side of the bed slate is part of the liquid metal filling and filtration system, with the filter housing being located directly beneath the sight glasses. The inverted hats in the

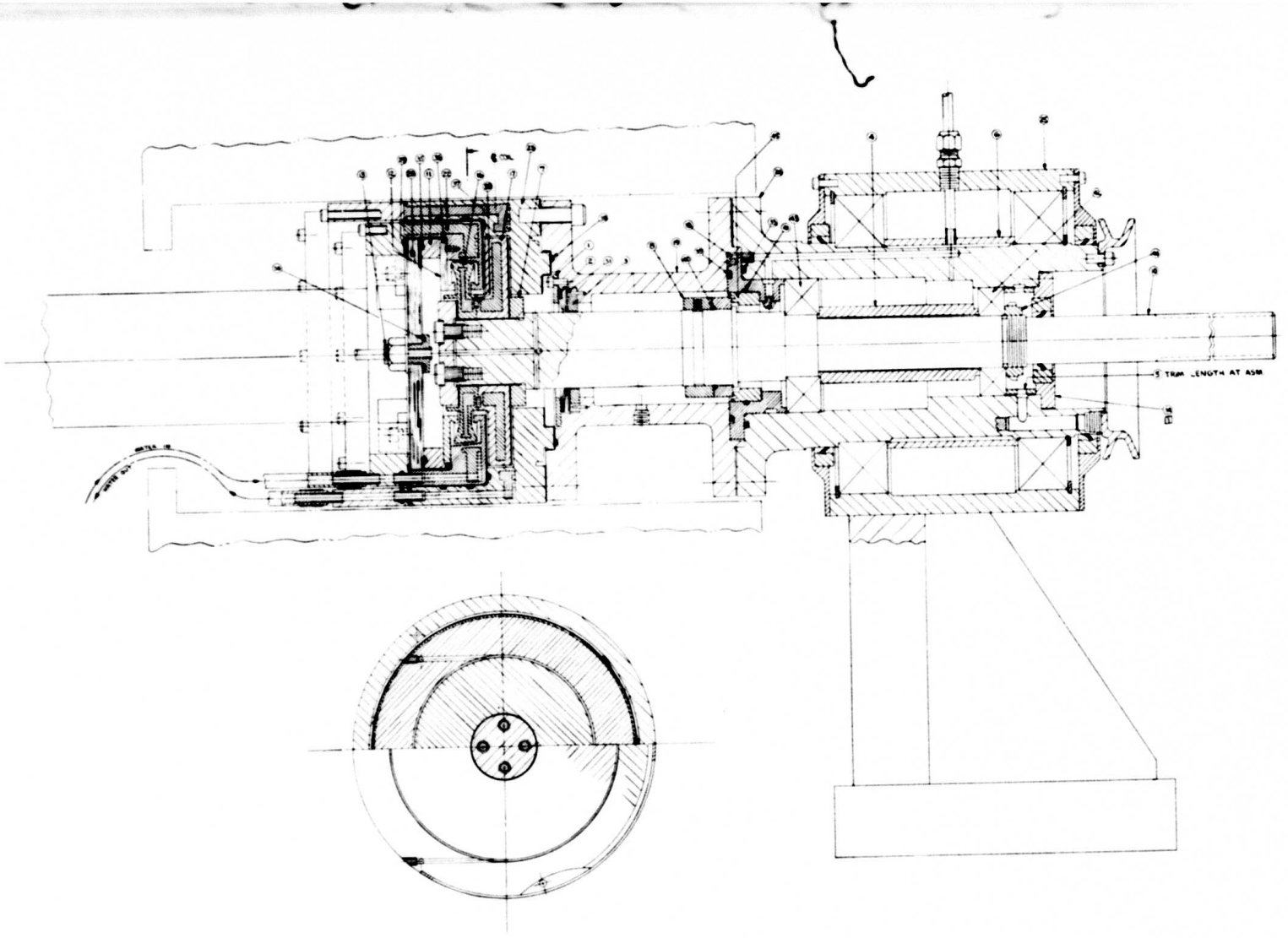

Figure 35. Current Collector Cross Section

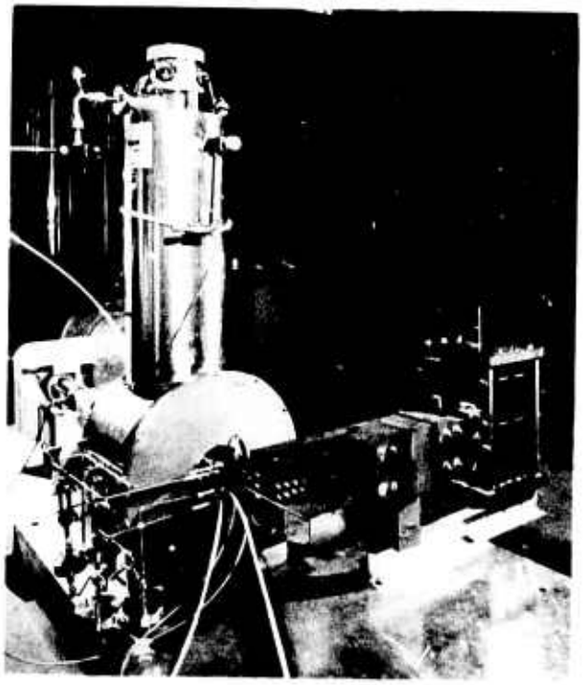

Figure 36. View of Terminal End

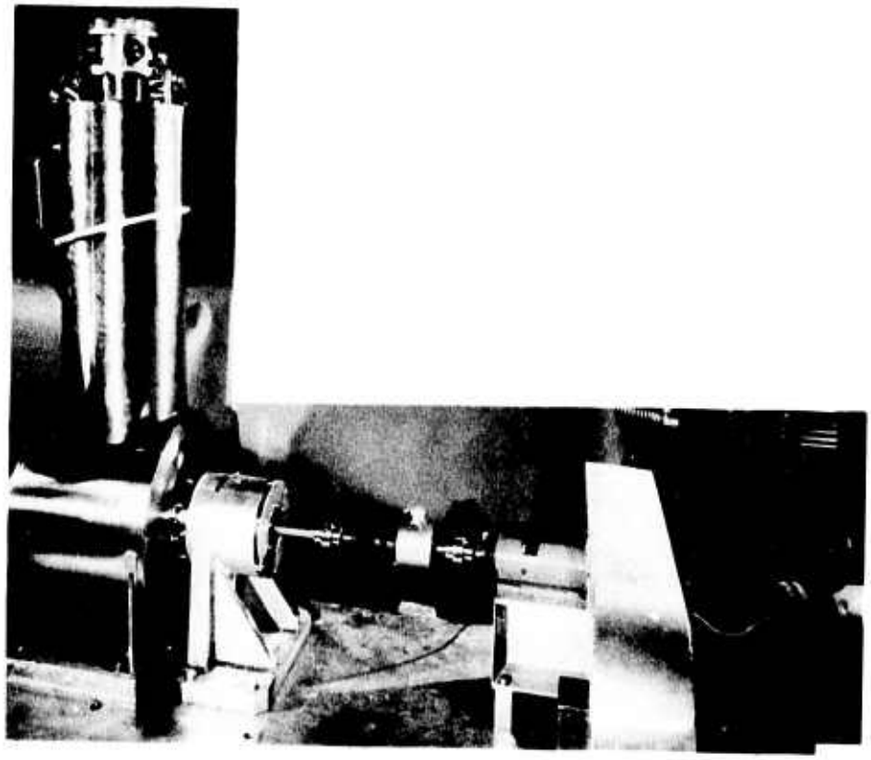

Figure 37. View of Drive End

lower corner are the housings of the welded metal bellows that control the liquid metal level in the generator. The plastic tubing entering the dewar bore provides cooling water to the generator and the water cooled portion of the bus. Approximately 6 inches inside the dewar bore is a glass window mounted on the end of the generator, through which can be seen the action of the liquid metal in the inner collector of the test rig.

The internal design of the test rig is shown in Figure 35. The rotor consists of two disks, an outer collector disk 6 inches in diamter and an inner collector disk 4.75 inches in diameter -- parts 17 and 16, respectively. The outer periphery of each disk is wetted with gallium, which completes the electrical circuit to the inner collector stator, part 22, and the outer collector stator, part 23. The radial thickness of the liquid metal circuit is 0.020 inch. The voltage, E, generated in this disk set is a function of the magnetic field strength, the rotational speed, and the diameters of the inner and outer disk, and can be calculated:

$$E = \frac{\pi NB}{60} (R_2^2 - R_1^2) \text{ (volts)} \qquad (18)$$

where:

B = Magnetic field strength (tesla)

N = Rotational speed (rpm)

R_1 = Inner collector radius (m)

R_2 = Outer collector radius (m)

This generated voltage causes a current to flow through the inner and outer collectors and through the rotor disks in series, and thence into the external bus bars that are attached to the concentric stator cylinders at their left-hand ends. Surfaces defined by a heavy line are electrically insulated (e.g., the outer surface of part 22, the outer surface of the shaft where it fits the bore of the rotor disks).

The left-hand end of the test apparatus is enclosed with a glass window (part 28), and the left-hand wall of the inner collector liquid metal trough (part 12) is made of polished transparent plastic; thus the action of the liquid metal in the inner collector can be observed during operation.

The outer members of the test apparatus have been described as stator members; however, examination of the bearing pedestal at the right-hand side of Figure 35 shows that these stator parts are actually supported on ball bearings; therefore, if the bus bars and fluid piping are disconnected, the stator assembly is capable of counter rotation with respect to the shaft. Such testing would be limited to open circuit and short circuit conditions, as operating with a load resistor would require another complete set of current collectors. In actuality, no contrarotating operation was done because it was found during

initial assembly of the apparatus that the bore of the solenoid dewar was badly out of round in its midportion. Radial clearance was therefore insufficient to allow rotation of the outer collector assembly. This is the reason the V-belt pulley shown on the right-hand side of Figure 35 does not appear in Figure 37. In place of the pulley, Figure 37 shows an annular plate that anchors the outer collector subassembly to the bearing pedestal housing (part 25 in Figure 35) in torsion.

A summary of the nominal design parameters appears in Table 15. A more detailed description of the various design elements is included in the following paragraphs.

Table 15

NOMINAL TEST APPARATUS SPECIFICATIONS

Characteristic	Specification
Speed	0-2200 rpm
Maximum power input	25 hp
Maximum load current	10,000 amperes
Voltage (at 3.0 tesla, 1800 rpm)	0.61 volt
Maximum field (approximate)	6 tesla
Inner collector diameter	4.75 inches
Outer collector diameter	6.0 inches
Collector width	0.6 inch
Collector radial gap	0.020 inch

BEARING, SEALS, AND COVER GAS SYSTEM

Both the collector rotor shaft and the collector stator are overhung from ball bearings mounted outside the dewar bore in the bearing pedestal. All parts, except the ball bearings and casual fasteners, are made from nonmagnetic materials (304 stainless or aluminum), in order to minimize the magnetic forces acting on both the ball bearings and the superconducting coil itself. Lubrication is accomplished by an oil mist system.

Mist is supplied through the 1/4-inch-diameter tube entering the top of the bearing pedestal and is ducted to the rotor bearings and the mechanical face seal mounted in part 18. This mechanical seal normally runs with air and lubricating oil on one face, and the collector system cover gas (dry nitrogen) on the other face. It would be exposed to the liquid metal only in the case of a gross spillover, or the slow migration of liquid metal in the form of dust or small droplets. The rubbing surfaces must be chosen to be compatible

with the liquid metal, however, and for this design the seal nose was made of carbon and the shaft mounted rubbing ring was faced with flame sprayed tungsten carbide. It should be noted that carbon seal surfaces are not usable in a NaK system.

The driven end of the rotor shaft is sealed by a lip seal mounted in part 14. The function of this seal is merely to divert the exhausting oil mist into a drain hole under the shaft, where it can be filtered to prevent fouling of the atmosphere in the testing area.

The collector test apparatus is fed with a high-purity nitrogen cover gas through a fitting (part 13) mounted in the center of the observation window. The cover gas blankets the liquid metal and has a positive flow path through the drilled end of the shaft, between the shaft and the inside diameter of the floating clearance seal (part 3) and hence out through a 1-psi check valve mounted in the drain hole in the bottom of the spool piece (part 19). When the shaft is at speed and gallium is in the collectors, the space between the two rotor disks could be sealed from the remainder of the internal volume. To prevent this, vent holes pierce the inner rotor disk.

The cover gas has several functions:

- The contaminants that diffuse through the outer O-ring seals are diffused and at least a portion of these contaminants are carried away before they react with the gallium.
- The slight positive pressure of the cover gas causes an outward flow through any small leak that may be present, rather than an inward leakage of oxygen.
- The outward flow of cover gas between the shaft and the clearance seal (part 3) prevents any oil or contaminants passing the main mechanical seal from entering the current collector spaces.

The clearance seal is made of carbon, with a 0.002-inch radial clearance from the rotor shaft. The carbon ring is pressed against the internal flange of the stator by wave washers, and it maintains its radial position only by virtue of its friction with the stator flange. In this way, the carbon ring automatically positions itself with respect to the shaft, and small radial clearances can be maintained without the necessity of having exceedingly close tolerances and stiff structures.

Cover gas was metered to the apparatus by maintaining a 40-psig pressure upstream of an orifice having a 0.005-inch diameter. This pressure resulted in a purge flow of approximately 0.7 ft^3/hr of dry nitrogen, which has a velocity of about 2 ft/s through the carbon ring clearance seal. This is a much higher gas flow than is actually necessary if the seals maintain their integrity. Boiloff gas from a liquid nitrogen dewar was used as the

cover gas supply. The oxygen content of this gas was measured to be in the range of 9 to 12 ppm. The water vapor content of the boiloff was not measured, but because the saturation pressure of water at liquid nitrogen temperature is approximately 10^{-17} torr, the water contribution from the liquid nitrogen is well below 1 ppb and therefore is of no consequence. Except for the final O-ring seal to the test apparatus observation window, the cover gas system was all metal to minimize contamination.

Further purification of the cover gas by bubbling through NaK was considered but not actually carried out, because it seemed unwarranted in view of the results obtained with the liquid nitrogen boiloff alone. Toward this end, experimentation was completed to obtain a good dispersion of N_2 bubbles in NaK (using water to model the liquid metal). By bubbling the gas into the liquid through a fine glass filter frit (4- to 4-1/2-micron pore size), a good bubble dispersion was obtained.

All O-rings used to seal the apparatus were made of Viton fluoroelastomer, to minimize oxygen and water vapor diffusion. When cooling water would have contacted a main enclosure O-ring, an extra O-ring was used to contain the water, and the space outside the main enclosure O-ring was vented to the atmosphere. Internal pockets where air could be trapped during assembly were avoided or vented. The apparatus was pumped down to less than 100-micron pressure and back-filled with the cover gas several times before the system was filled with gallium.

ROTOR AND STATOR

The initial problem to be answered in the design of the interior of the gallium test apparatus was the choice of materials in contact with the liquid metal. Copper, ideal for use in NaK current collection systems, is not acceptable for long-term use with gallium. Metals that are highly compatible with gallium are niobium, tantalum, molybdenum, nickel, austenitic stainless steels, and inconel. Of this group the most practical from the standpoint of cost and availability are nickel and austenitic stainless steel. The relative electrical resistivity of the metals under consideration is shown in Table 16.

Due to its high resistivity, stainless steel should only be considered as a cladding over copper for high-density propulsion motors. Nickel is marginal in this respect, but because nickel is a ferromagnetic material, its use in the test apparatus would cause additional magnetic forces on the superconducting coil. It was decided to avoid any additional coil forces and thus to consider only the potential of nickel as a coating over a bulk substrate.

Although electroplating of nickel seems obvious, it is very difficult to obtain uniform coatings of electrodeposited nickel over complex shapes. There are strong tendencies for heavy granular deposits to be made on outside corners, while holes and undercuts are starved. Such nonuniform coatings

Table 16

COMPARATIVE RESISTIVITIES

Material	Relative Resistivity
Copper	1
Gallium	16
Nickel	5.5
Austenitic Stainless Steel (304)	42

would be of low dependability as protection against gallium attack. Nickel, however, can also be deposited on metallic substrates by electroless plating processes. One of these is the Kanigen process that is regularly used to apply corrosion protection to the insides of tanks and chemical processing equipment. It has the ability to uniformly plate complex shapes having deep undercuts and holes. The deposited layer, however, is not pure nickel. A small percentage of phosphorus is also present, and to determine the compatibility of these coatings with the gallium sample, Kanigen platings were obtained on substrates of copper, aluminum, and low-carbon steel.

These samples were electroplated with gallium to ensure wetting, submerged in liquid gallium, and held in an oven at 100° C. After two weeks of exposure, patches of dullness were evident on the original luster of the wetted surfaces. Inspection showed that small pits and mounds had developed in all samples, and a few crystallite blocks had formed with dimensions up to about 0.025 inch. Qualitative analysis of these blocks showed them to be gallium-nickel compositions. This showed the unsuitability of such a plated surface and cast some doubt on the suitability of solid nickel, but because it was decided to concentrate on stainless clad copper, no further work was done with nick l in any form.

Many hundreds of hours of running time of a solid stainless steel wheel in gallium during the course of another investigation had indicated excellent tolerance of AISI 304 steel for the liquid metals; thus after the poor showing of the nickel plating it was decided to construct the current conducting elements of the test apparatus from stainless clad copper. The first approach was to cast the copper core directly into stainless steel shells and weld on stainless steel cover plates on surfaces through which current did not pass. Accordingly simple test samples of 304L stainless steel were made to duplicate the essential casting problems of the rotor and stator, the most difficult piece being a sample of the stator structure in which it was required to cast cylindrical cores of copper that were 9/32 inch in diameter by 2-1/2 inches long. The technique followed was to insert machined slugs of copper into the machined stainless steel cavities and place the assembly in a hydrogen furnace to melt the copper. The assembly was then withdrawn and the

eopper was allowed to solidify. Because the melting temperature of copper is suffieiently high to ensure the reduetion of oxides on the surface of the 304L stainless steel, exeellent wetting of the steel by the eopper was achieved in all trials. In the deep holes described above, gross porosity of the copper beeame evident after seetioning the test samples.

Further test samples were prepared having larger eavities at the top of the 2-1/2-inch-deep holes, in order to provide a larger reservoir of molten eopper to the holes during solidifieation, but adding up to an inch of exeess head had no significant effeet on the degree of porosity. Investigating the possibility that the porosity might be due to dissolved hydrogen in the copper eoming out of solution during solidification, samples were also processed in a vaeuum furnaee. This degassing did not improve the porosity and due to the press of time, the casting program was stopped in favor of bonding the eopper and stainless steel by brazing. Toward this end, samples were prepared using gold-nickel euteetie braze alloy (melting temperature = 952°C), and excellent results were obtained in a hydrogen furnace. The test apparatus was therefore made using this technique.

The details of the stainless elad copper design can be seen by examining Figures 38 and 39, where the cross seetions of the inner collector rotor and stator are shown. Figure 38 shows that the rotor disk comprises three elements:

- Main stainless steel shell, which forms the bore, the periphery, and the right-hand side (this is the side that clamps against the outer eollector rotor disk)
- Copper core
- Stainless steel cover plate enclosing the left-hand side of the disk

The copper insert is brazed to the main shell. The cover plate is not brazed to the copper; brazing is unneeessary because no eurrent crosses the eopper/cover plate interface.

The manufaeturing sequence is to rough-machine the steel shell and eopper insert, braze, finish-maehine matching faces of the eover and disk composite, electron-beam-weld the eover to the shell, and finish-maehine. The current path in the stainless steel is quite short and the stainless steel thiekness at the wheel periphery could readily be cut in half from the 0.090-inch thiekness of this design. The manufaeturing proeedure for the stator seetions is essentially the same as that deseribed above.

The axial current path is not a continuous eopper ring but a series of axial eopper slugs terminating on an exposed eopper ring on the left-hand face. This exposed face is on the outside of the apparatus and is not exposed to the liquid metal. It was made eopper rather than stainless steel to minimize eontaet resistanee with the external current bus that attaches to this

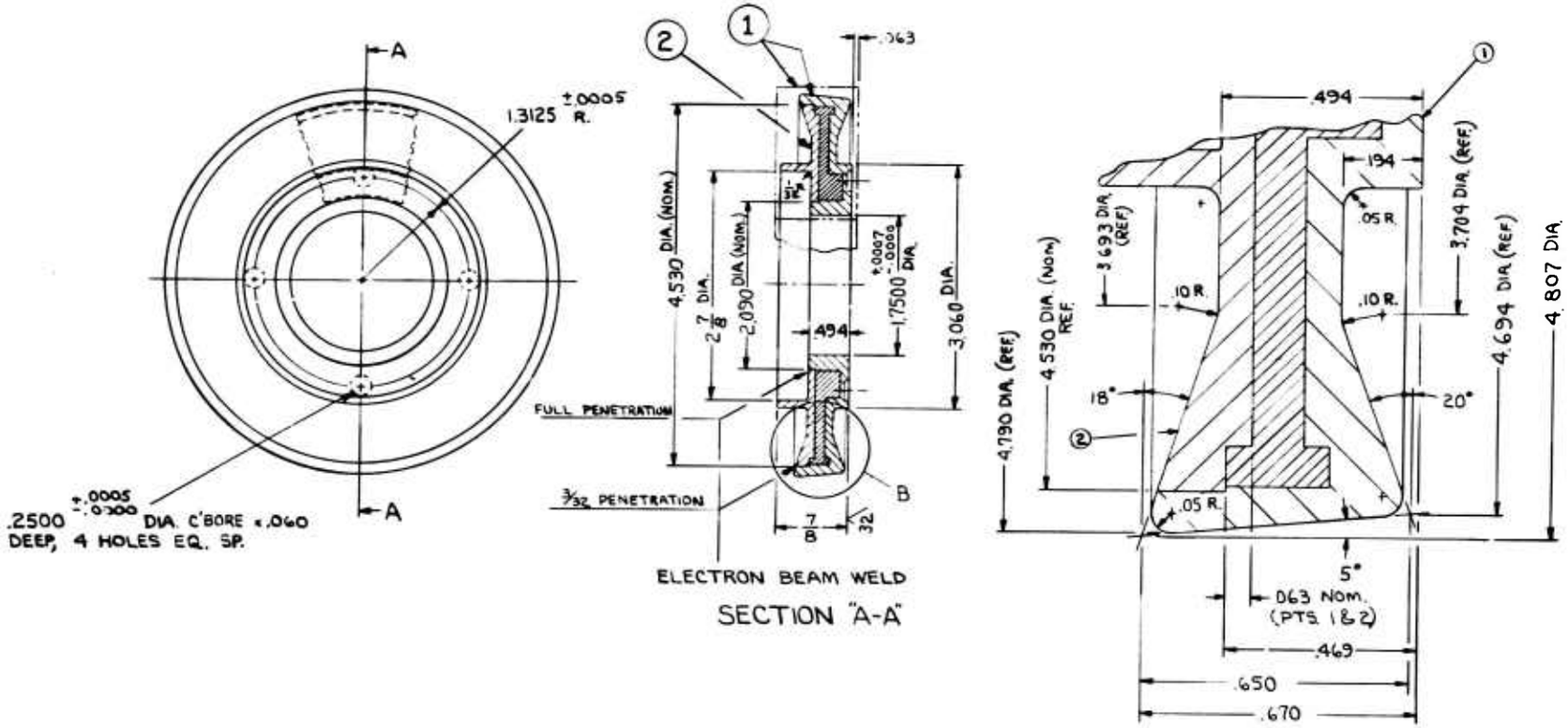

Figure 38. Cross Section of Rotor

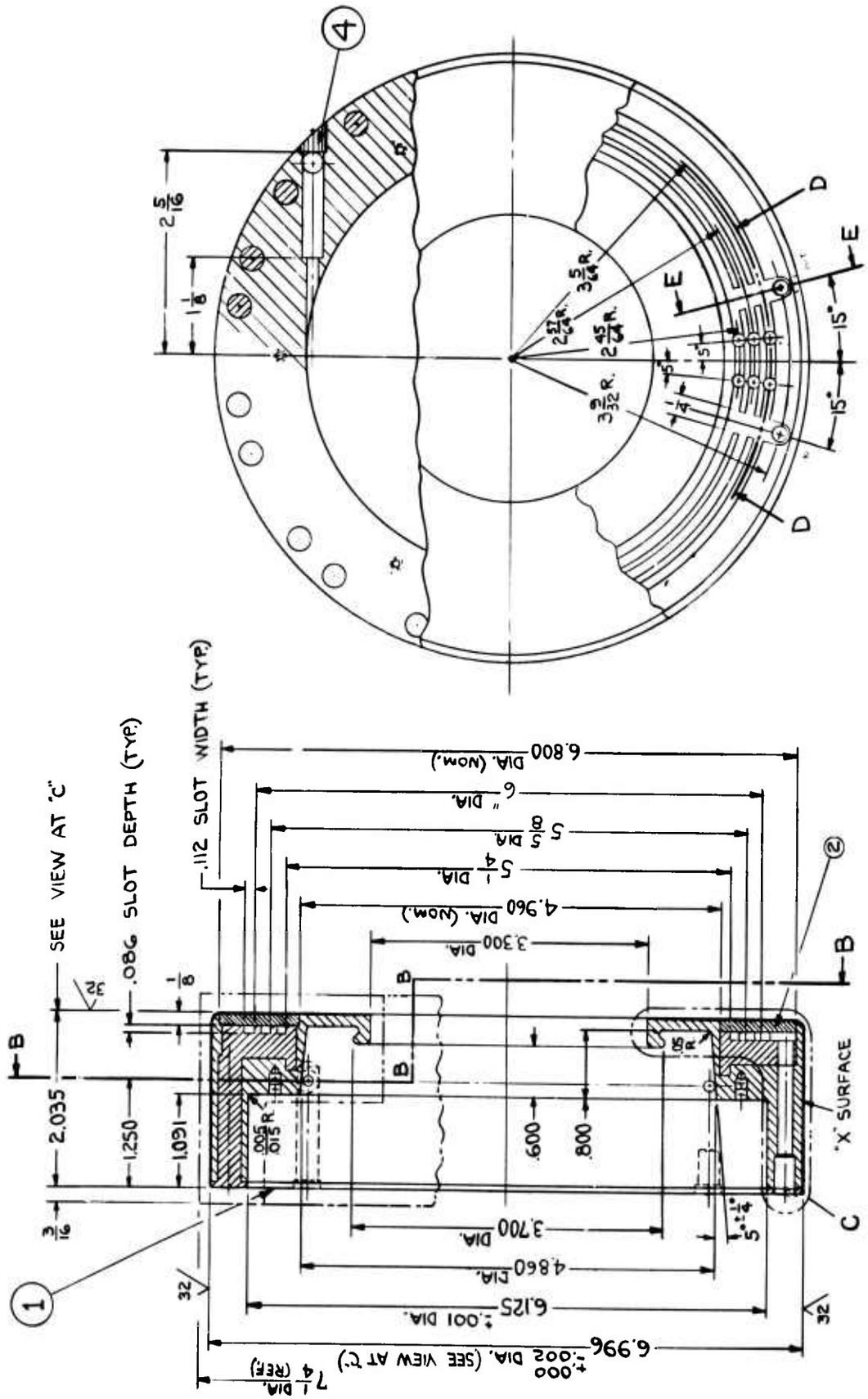

Figure 39. Cross Section of Stator

surface. On the right-hand face of the copper insert, under the cover plate, annular passages are machined to permit direct water cooling of the apparatus.

A potentially high-resistance joint exists at the interface between the inner collector rotor disk and the outer collector rotor disk. If these two stainless steel surfaces were in direct contact, an extremely high clamping force would be required to obtain an acceptable contact resistance. To eliminate this problem, the mating faces of the two disks were first electroplated with gallium and the disks were assembled at a high enough temperature to melt the plated gallium, producing a soldered joint. The four shallow holes in these mating surfaces are for the insertion of short stainless steel plugs that act as keys to transmit torque between the two rotor disks. The peripheries of both rotor disks and the mating inner surfaces of the stators were also electroplated with gallium before assembly, in order to ensure good wetting and negligible contact resistance between the steel and the gallium.

The width of the rotor disks was chosen to yield an average collector gap current density of 1000 A/in^2 at a load current of 10,000 amperes. The inner collector disk necks down to a narrower section, giving a hammerhead cross section. This design gives sufficient pool volume for all of the liquid metal required for filling the gap to remain in the collector well when the disk is not rotating. It also allows the placement of the gutters of part 12 of Figure 35 and of Figure 39 in a more advantageous position to capture the liquid draining from the periphery of the disk and thus confine it.

The rim of the inner collector rotor disk has a slight cone angle, so in the case of liquid loss, less liquid is required to maintain electrical continuity across the gap. The outer collector rotor disk, due to its larger diameter, did not require any additional pool reservoir volume and for simplicity it was made as a flat disk.

The internal resistance of the above design was calculated to be 7.2×10^{-6} ohms, of which 4.1×10^{-6} ohms was in the rotor disks and 3.1×10^{-6} ohms was in the stator circuits. The gallium resistance amounted to 0.044×10^{-6} ohms. After the initial assembly of the apparatus, the internal resistance was measured to be approximately 8.5×10^{-6} ohms with the shaft rotating and the collectors having a full charge of gallium. The discrepancy is felt to be within the accuracy of the calculations.

The electrical insulation between the two stator sections, and isolating the rotor disks from the shaft, is flame sprayed alumina filled with epoxy resin and ground to size. This is a durable, dimensionally stable insulation system that has been proven effective with NaK current collection systems.

Figure 40 shows a partial assembly of the apparatus, the inner and outer rotor disk being mounted on the left-hand end of the shaft but not yet clamped in place by the end cap of the shaft. Figure 41 shows the inner collector and

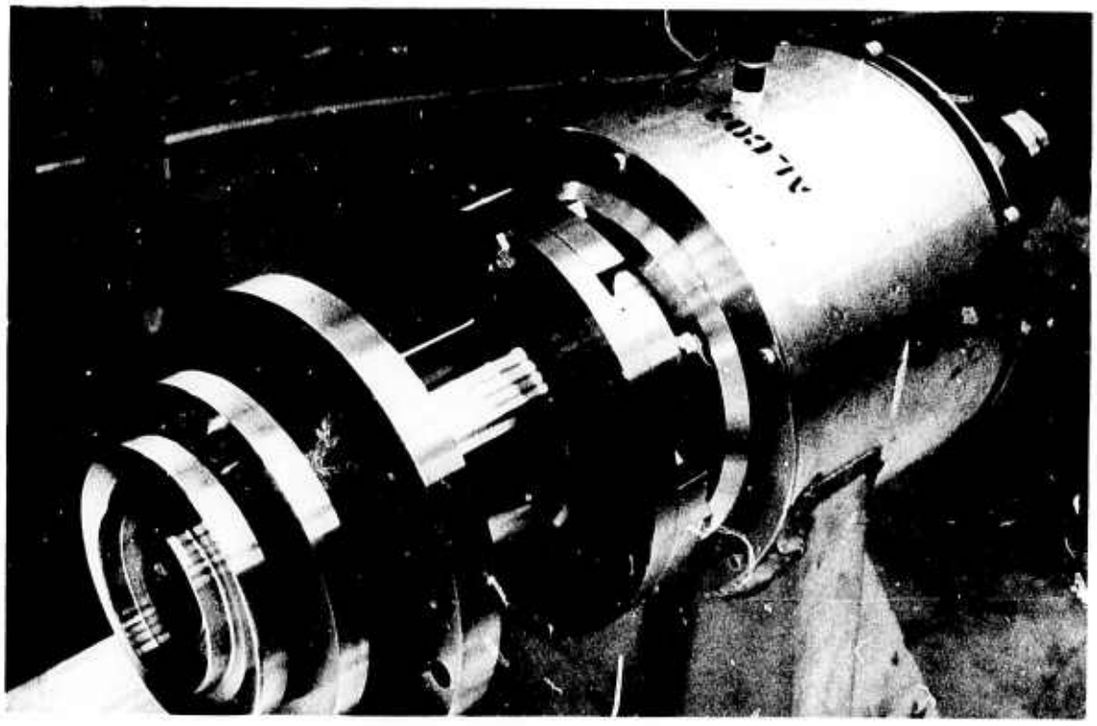

Figure 40. Rotor Assembly

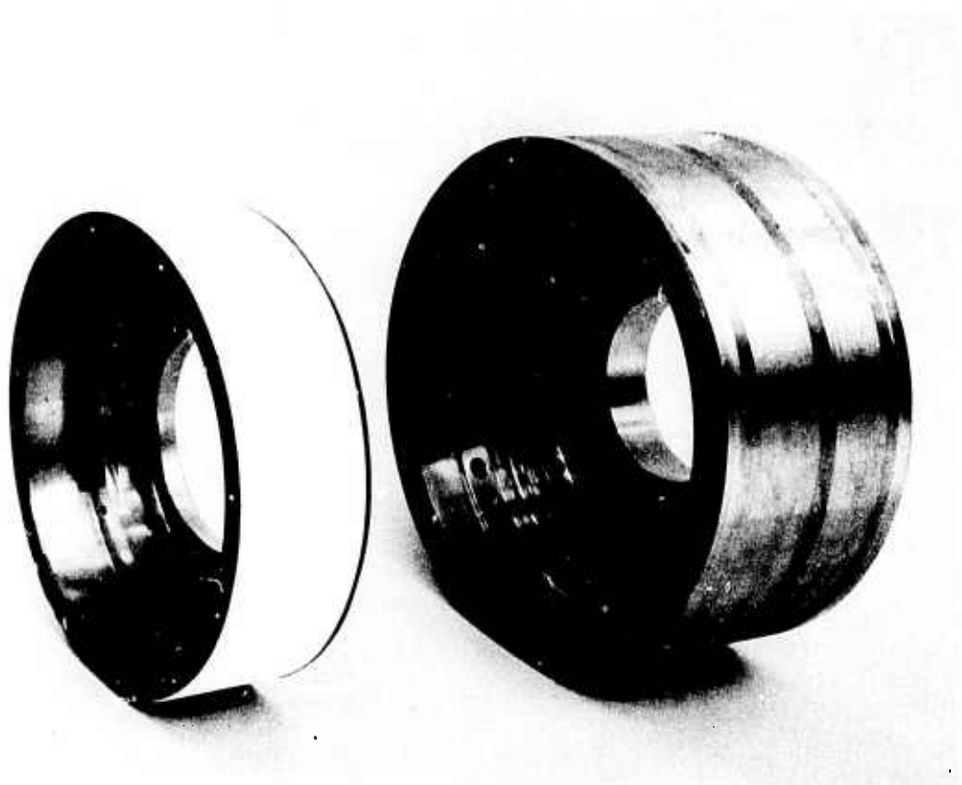

Figure 41. Inner and Outer Stator

outer collector stators. The tangential holes visible in the bores of both pieces are the fill and circulation ports for the liquid metal. There are two such holes in each piece, located as shown in Figure 39.

LIQUID METAL HANDLING

The design requirements of the liquid metal handling system are to allow the proper filling and level regulation of the gallium in the collector spaces and to provide for the filtration of the gallium during collector operation to remove any oxides or other solids that might form. A schematic diagram of this subsystem is shown in Figure 42 (both the inner and outer collectors have separate systems). Although not indicated in this figure or in Figure 36, the temperature of these systems was regulated to approximately 95°F by heating tapes and thermal insulation.

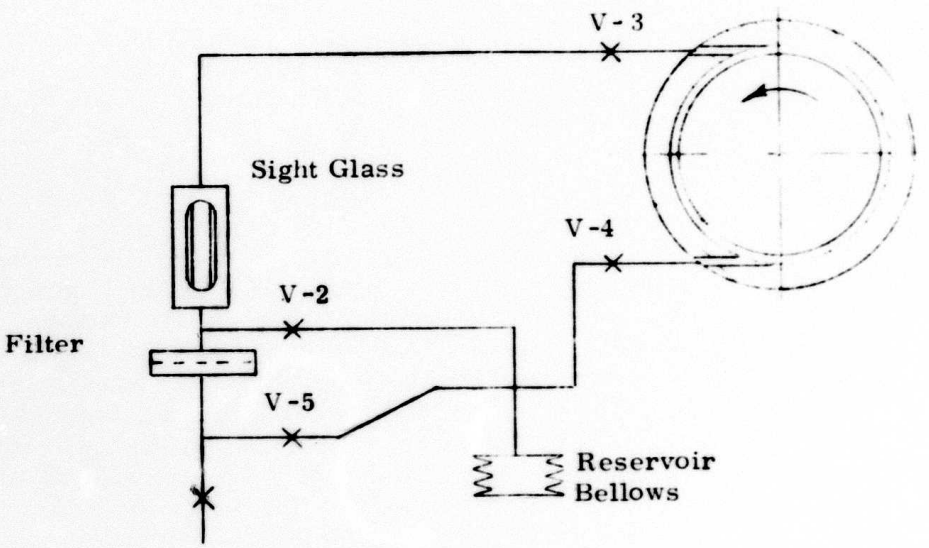

Figure 42. Gallium Handling System

The system was designed to be operated in the following manner:

1. Initial Filling and Level Regulation. With valve V-1 closed and all other valves opened and the reservoir bellows compressed to minimum volume, the entire collector system was pumped down with a mechanical vacuum pump, to a pressure of approximately 40 microns. A tube extending from the bottom of valve V-1 was submerged in a flask of molten gallium and valve V-1 was slowly opened, drawing the liquid metal into the bottom of the system until it was just visible in the bottom of the sight glass. The reservoir bellows was then expanded, while allowing more liquid to be drawn through valve V-1 until the entire volume

of the bellows (about 30 cc) was filled and the level was still visible in the sight glass. Valve V-1 was then closed. The liquid metal level in the collector spaces was then controllable by varying the volume of the bellows, with the level of the collector pool being gauged by the level in the sight glass.

2. Filtration. Liquid metal circulation through the filtration loop is accomplished by tapping off the dynamic head of the fluid in the collector gap, the circulation being from the top to the bottom of the filter. Valves V-2 and V-5 allow bypassing of the filter. Valves V-3 and V-4 allow isolation of this subsystem from the collector itself. The filter element used was a glass frit of 4- to 4-1/2-micron pore size (designated "fine"). By separate tests it was determined that the flow of liquid gallium (95° to 100°F) was initiated through this class of filter at a head height of less than 1 foot, which is equivalent to a velocity of 8 ft/sec or less. At 1000 rpm the peripheral velocities of the inner and outer collector wheels are 21 ft/sec and 26 ft/sec, respectively.

Except for the sight glass and the filter element, both of which were sealed with O-rings, the liquid metal handling system was completely stainless steel.

COOLANT SYSTEM

The temperature of the gallium collector was maintained by circulation of water through the stator cooling channels visible in Figures 35 and 39. The water is in direct contact with the current carrying copper inserts of both stators and thus the full terminal voltage is impressed across the water; however, the resistivity of the tap water used as coolant was measured and was found to be high enough to make this short circuit current completely negligible. The coolant system consisted of a positive displacement pump and sump tank that maintained a closed circuit water flow into the collector stators and back to the sump. The minimum temperature was controlled by a thermostatically regulated electric heater to 110°F. When losses within the collector test apparatus increased the temperature, the heater turned off and cool makeup water was admitted to the sump tank by a syphon controlled water valve. The excess water drained from an overflow in the sump tank. In this way the water temperature in the cooling passages of the test apparatus was maintained in the range 110° to 115°F at all times.

OTHER TEST EQUIPMENT

Torque input was measured by a shaft mounted resistance strain torque sensor (BLH type A-1, 1000 in-lb) reading out through a Daytronic type 91 strain gage transducer. Shaft speed was measured by counting the pulse output of a 60-tooth shaft mounted gear with a Hewlett Packard Type 5321-B electronic counter. Terminal voltage was measured by a Keithley 160 digital

voltmeter, and load current was measured on a 20,000-ampere shunt. The load resistance consisted of a serpentine sheet steel ribbon submerged directly in cooling water; this is the box structure visible at the right-hand end of the bus bar shown in Figure 36.

PRELIMINARY AND OPEN CIRCUIT TESTS

LIQUID METAL BEHAVIOR

Initially only valves V-1 (the drain valve) and V-2 (the filter bypass valve) of the gallium handling system were in the loop, but subsequent tests showed the need for additional liquid control, and the other valves were added.

Because only the inner collector cavity was visible in the test stand, sight glasses were included in both the inner and outer collector loops to be used to determine the static, pooled height of the gallium in each collector. During initial calibration tests with water, correlation between the sight glass and the collector cavity was excellent, but when the water was replaced with gallium, the results were quite different. With the inner collector loop charged with gallium, the reservoir bellows was compressed to add liquid to the collector cavity.

No correspondence between the sight glass and cavity level was observed. The sight glass was nearly filled before any gallium was seen in the cavity. A similar event occurred in attempting to fill the outer collector cavity. In both cases, the gallium did not react linearly with the attempted adjustment. It appeared that a driving pressure large enough to overcome the gallium surface tension was required before flow would occur, and then the flow would surge into the cavity. Once a pool was established in the cavity, its level did, however, change linearly with bellows adjustment.

Because of the problems associated with the static filling, dynamic filling was attempted. The shaft was rotated by the drive motor and the gallium was added by compressing the reservoir bellows. No magnetic field was present and no current flowed in the disk. The suitability of the liquid level was judged by the quality of the film at the rotor tip and by the flow in the loop, as seen in the sight glass.

Filling the collector cavities was more easily achieved, holding the gallium volume in the loop constant, at higher shaft speeds where higher centrifugal pressures caused the liquid to flow. Once gallium was in the collector and the rotation stopped a liquid pool would form.

As the shaft was accelerated, two types of flow instabilities were noted in the rotor tip film. First, below a certain speed gravity effects predominated and full filling around the wheel periphery was prevented. In this situation, liquid would start to climb up the rotor periphery in the direction of

rotation, but would then fall back into the pool. A velocity of 500 rpm had to be achieved before a full tip film was achieved and this spilling back ceased.

The second instability noted occurred at the top of the disk. As the volume of liquid metal in the collector was increased, while holding the wheel velocity constant, the film at the top of the rotor was seen to pulse axially and eventually tumble over the side of the rotor. At higher wheel velocities, more gallium volume was required to achieve this instability.

The first phenomenon indicated that centrifugal forces at low speeds were not enough to overcome gravity and lift the gallium from the pool and around the periphery. The second instability resulted when the centrifugal forces were not enough to maintain the larger volumes of liquid in the gap and spillage over the disk side occurred.

At minimal gallium volume settings, where a full film was achieved, higher speeds were required to achieve flow in the handling loop as viewed through the sight glass. As the liquid volume increased, flow in the handling loop was achieved at lower shaft speeds. Enough centrifugal pressure to cause flow in the loop had to be obtained by increased speeds or increased liquid mass before flow would occur.

The effects of the in-line filter on the loop flow were observed while opening and closing the bypass valve, V-2. With the valve closed, all the loop flow had to go through the filter and was subjected to the flow impedance associated with the filter. When the bypass was closed, the flow rate was seen to decrease and at higher shaft speeds or liquid volumes, the flow was seen to back up into the sight glass. This phenomena did not occur with the bypass valve open. At no time, however, did the filter clog or evidence any increased resistance to the flow of fluid. Flow was restricted through it due to the filter's natural resistance.

With a magnetic field added, but no current flow (open circuit tests), the following observations regarding gallium performance were made:

- Increasing the liquid metal volume in the collectors allowed the loop flow to be achieved at lower shaft speeds, but also increased the speed at which the gap film was stable. These results are consistent with earlier findings.
- As the magnetic field strength was increased, higher rotor speeds were required to achieve liquid flow in the loop.
- With increased field strength, the liquid in the rotor gap became less stable. The tumbling phenomena occurred at higher speeds with higher field strengths. Higher centrifugal pressures were required to control this instability. In addition, with the field strength at about 4 tesla, gallium particles appeared to streak across

the face of the rotor from one side to the other. This streaking appeared unrelated to the tumbling instability.

During the load tests, with both magnetic field and the resulting current flow, the gallium reacted differently. During initial testing with the magnetic field at about 3 tesla, the gallium in the inner collector disappeared and electrical arcing occurred. Attempts were made to add more gallium, but it would not stay in the rotor tip gap, and arcing continued. When the shaft was stopped, no gallium pooled in the collector cavity. After dropping the magnetic field, a pool of liquid metal that had been trapped in the handling loop appeared.

In order to retain the liquid in the collectors, additional valves V-3, V-4, and V-5 were added. With these valves, the collector could be isolated from the handling loop and the bellows could be isolated so that added gallium could flow to the collector cavity only.

While the testing was stopped to add the valves, the test assembly was torn down and inspected, and gallium was found to have spilled into the cavity behind the outer collector. In an attempt to minimize this spillage, the assembly changes shown in Figure 43 were made. The spacer (part 1) behind the outer collector disk was modified to act as a liquid slinger. The outer collector stator (part 2) was modified as shown to trap the liquid in the rectangularly shaped annulus and direct the liquid back to the collector cavity through a slot at the bottom of the annulus. A groove was machined in the

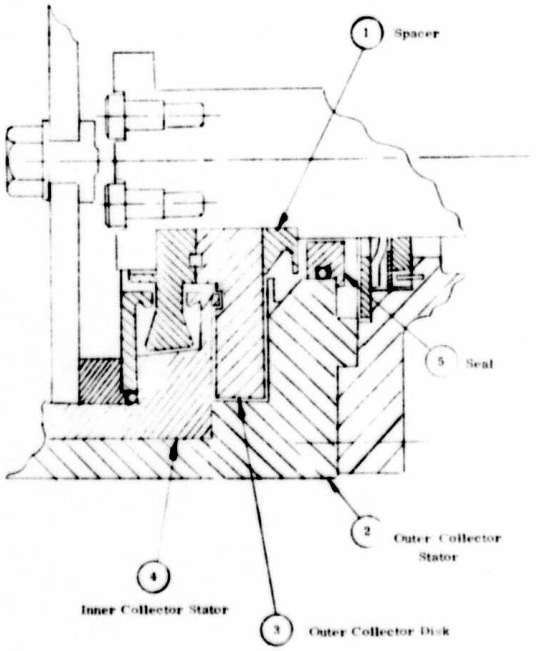

Figure 43. Test Assembly Modification

outer collector rotor (part 3), to serve as a clearance space for the baffle ring mounted on the intereollector ring (part 4). This baffle was to prevent migration from the outer to the inner collector cavity during rotation. An additional seal (part 5) was added to prevent leakage along the shaft. This piece formed a positive seal on the stator, but relied on a close clearance with the rotating shaft for sealing at its inside diameter.

During continued load tests, no further arcing at the inner collector was seen, but there were indieations of areing in the outer collector. This situation occurred when high load currents were produced by high disk speeds in the magnetic field. With the rig acting as a generator, the outer collector disk rotates in a direction opposite to the tangential Lorentz force produced in the liquid by the load current and the magnetic field. The result is that a drag causing spillage and splattering of the liquid metal results. At the higher speeds, in relatively high magnetic fields, this effect was evidently large enough to empty the outer disk gap and cause arcing. This arcing was evideneed by rumbling and erratic load current readings. These speeds were avoided during subsequent testing.

At low speeds, during the load tests, the gallium was visibly unstable in the inner collector, and significant tumbling and splattering similar to that previously described took place. A significant buildup of gallium was seen in front of the front baffle plate, as a result of the splattering from the inner collector.

In general the load tests were limited to intermediate speed ranges by the fluid performance. At low speeds instability such as the liquid tumbling seen in the inner collector occurred, while at high speeds the gallium was ejected from the outer collector gap by the reaction of the load current and the magnetic field.

LOSSES ON ELECTRICAL TESTS

Before charging the collector system with liquid metal, a test run was made to determine the friction torque due to bearings, seals, and windage. The friction torque was measured to be substantially constant at 0.5 ft-lb over the entire speed range, as shown in Figure 44.

With the system charged and rotating, internal resistance of the test rig was measured by running currents in the range of 100 to 1500 amperes from a separate power supply and with zero field excitation. In this current range and over the speed range of 1200 to 1800 rpm, the terminal-to-terminal internal resistanee measured an average of 8.5×10^{-6} ohms with no observable dependence on either speed or current. These measured values were in substantial agreement with calculated design values of internal resistance. During later operation of the current collector with field excitation, internal resistances up to 40×10^{-6} ohms were measured. The zero field excitation tests

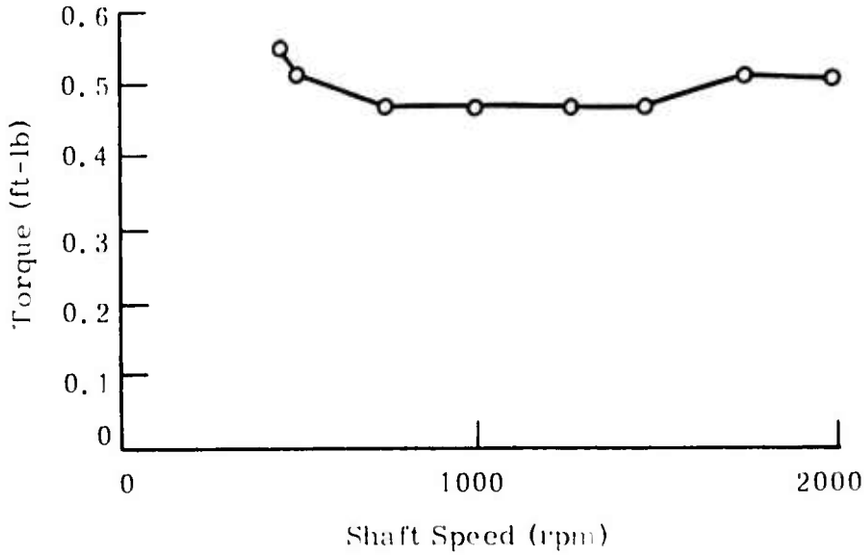

Figure 44. Bearing and Seal Torque

were then repeated, and the 8.5×10^{-6} ohms was found to have increased to 12×10^{-6} ohms.

With the superconducting solenoid excited and the liquid metal system charged, open circuit voltage was measured as a function of field excitation and rotor speed. These data allowed the calculation of internal resistance during subsequent load testing and also calibrated the effective magnetic flux density of the superconducting solenoid. The effective flux density is defined by:

$$V = \frac{B\pi}{60} (R_o^2 - R_i^2) N \qquad (19)$$

where:

B = Effective flux density (tesla)

N = Rotor speed (rpm)

R_i = Inner collector disk radius (m)

R_o = Outer collector disk radius (m)

V = Generated voltage (volts)

In the collector test rig, which is an acyclic generator, the open circuit voltage is equal to the generated voltage under load conditions, because there is no armature reaction. The field calibration is shown in Figure 45 in terms of both generated voltage and effective flux density.

The measurement of drive torques during the open circuit testing allowed the calculation of collector losses. These losses are plotted in Figure 46

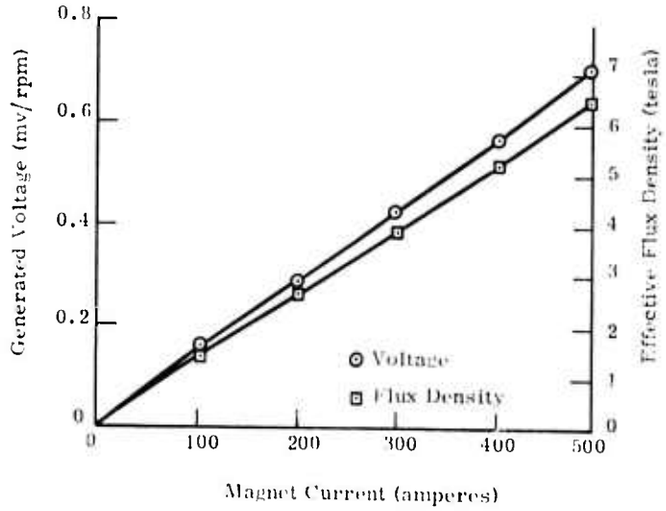

Figure 45. Open Circuit Voltage

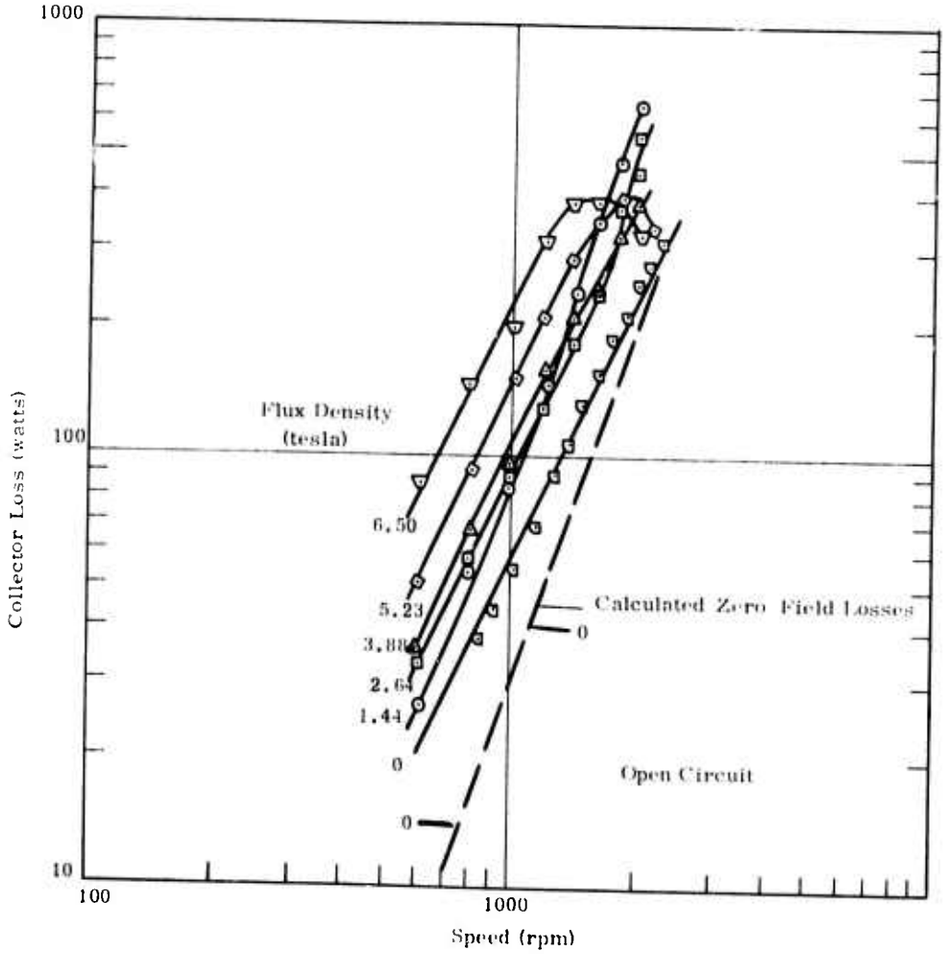

Figure 46. Open Circuit Collector Loss

from approximately 600 to 2200 rpm and from 0 to 6.5 tesla effective field strength. The lower test speed was limited to the point where visible tumbling of the gallium was incipient and the upper speed was the limit of the drive motor. The maximum magnetic flux density is the result of a superconducting solenoid current of 500 amperes, which was previously established as the upper practical limit of superconductor current.

It would not be unexpected if the losses were proportional to the cube of the speed, particularly at low flux densities where a typical turbulent flow condition would seem to obtain. The dashed line in Figure 46 is a plot of calculated zero-field losses based on correlations of long concentric cylinders with small annular spacing (Ref. 4). This calculated loss is very nearly a cubic with the speed (as indicated by the 3:1 slope on the log-log plot) while the zero-field data points lie nearly on a 2:1 sloped line indicating a speed squared relationship. This would be typical of a laminar flow situation; however, the Reynolds number based on radial gap thickness is well into the turbulent regime, and no magnetic field is present on the lower line of data to suppress turbulence. (The gap Reynolds number at 1000 rpm is 12,800 at the periphery of the inner collector.) Note that the experimental data are higher than the calculated data in the speed region tested, but the two lines cross at approximately 2300 rpm.

When the magnetic field is applied at the level of 1.44 and 2.64 tesla, the data show a tendency to approach a cubic relationship with speed, at the higher speeds. At the higher field strengths, however, this cubic tendency is suppressed and the loss curves reach limiting values of approximately 400-watts. Because the periphery of the inner collector is not quite parallel to the applied magnetic field, eddy currents are generated that are part of the measured losses. When calculated by the methods of Reference 1, a value of 15.3 watts of eddy loss at 1000 rpm and full field excitation is obtained. This is a very small part of the observed effects.

In Figure 47, a cross plot of the above loss data is made at a constant speed of 1000 rpm, both for this open circuit test and for later test results where load currents up to approximately 5500 amperes were flowing. This plot shows a tendency for the open circuit losses to follow a B^2 law at the higher flux densities and before the losses reach the peaking tendency shown in Figure 46.

LOAD TESTS

Subsequent to the open circuit testing, the load resistance was connected across the output bus and a series of load tests was run at three settings of the load resistor. The range of variables tested is summarized in Table 17. The dimensionless variable, δ, is a measure of the ratio of electromagnetic forces to dynamic force acting on the liquid metal and is defined as (see Appendix I, "Current Collector Gap Losses"):

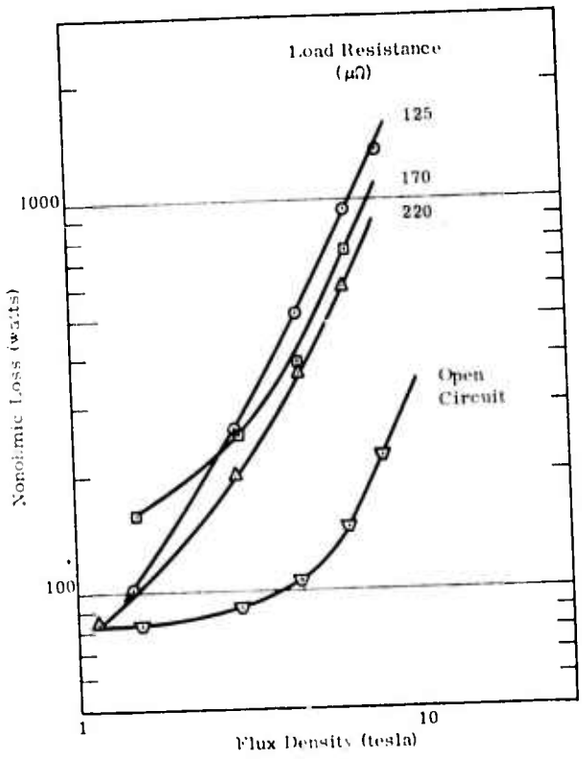

Figure 47. Collector Loss (Speed = 1000 Rpm)

Table 17

SUMMARY OF LOAD TEST PARAMETERS

Load Resistance ($\mu\Omega$)	Maximum Load Current (amperes)	δ_{min}	δ_{max}	B_{min} (tesla)	B_{max} (tesla)	Internal Resistance ($\mu\Omega$)
220	4480	0.012	0.71	1.12	5.2	12-30
170	5520	0.012	0.68	1.45	5.25	15-40
120	5340	0.033	2.32	1.40	6.5	21-39

$$\delta = \frac{2BJd}{f_\rho V_o^2} \qquad (20)$$

The test apparatus was designed with the intention of exploring a much wider range of variables than those shown in Table 17; however, operational limits were encountered upon operation of the equipment. Low speed was limited by the instability of the liquid metal in the gap; the speed required to maintain a continuous ring of gallium in the collector gap being higher than

expected. This limited the maximum value of δ obtainable. High speed at high-field strength was limited by erratic behavior of the electrical conductivity of the gallium filled gap and by the more rapid migration of the liquid metal out of the collector spaces. This was made evident by erratic variations of the load current, torque, and terminal voltage at higher values of speed and field strength. This erratic behavior deteriorated rapidly, and within minutes major load variations were occurring with arcing in the collector gap.

This cycle of deterioration was completed in a matter of minutes at the highest flux densities at speeds above 1500 rpm. Migration of the gallium was more rapid from the outer collector, but liquid loss occurred from both collectors.

During this erratic operation, the internal resistance of the collectors went quite high, due to the loss of conducting fluid. When the lost liquid was restored and the apparatus operated in a stable region, the internal resistance was still higher than that measured during the preliminary tests. The wetting of the collector surfaces had deteriorated, leading to the higher values of resistance listed in Table 17. No relationship was evident between these variations of internal resistance and either speed or field strength.

Current collector losses, exclusive of the I^2R contribution, for this series of tests are plotted in Figures 48 through 50. As in the open circuit tests,

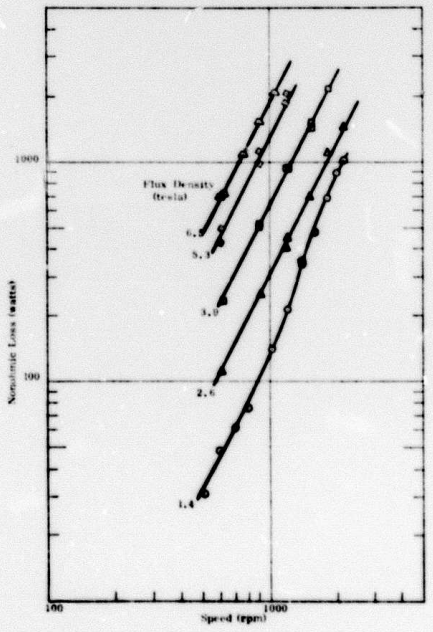

Figure 48. Collector Loss (R_{Load} = 120 μΩ)

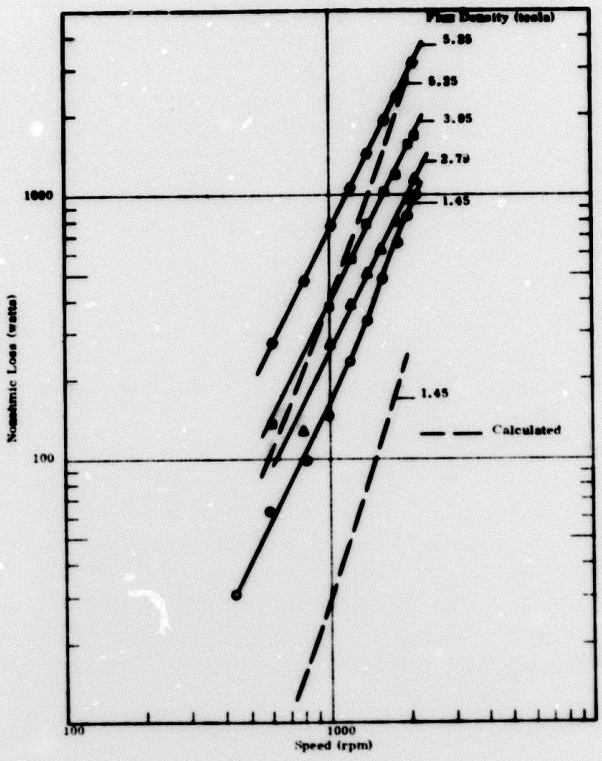

Figure 49. Collector Loss (R_{Load} = 170 $\mu\Omega$)

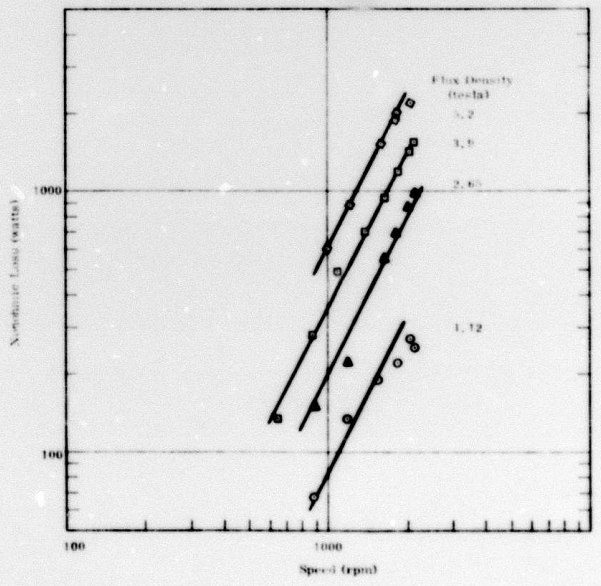

Figure 50. Collector Loss (R_{Load} = 220 $\mu\Omega$)

the data points are well represented by a line having a two-to-one slope indicating a speed squared relationship. Losses calculated following the flooded collector analysis of Reference 3 are shown as dashed lines on Figure 49 for the cases of the lowest and highest field strength. It is evident that the analysis, which has been found to adequately predict flooded collector losses, does not properly describe the loss phenomena in the nonflooded case.

A cross plot of the above loss data at a constant speed of 1000 rpm is shown in Figure 47. As with the open circuit case, this plot shows a strong tendency for the losses to follow a B^2 law. This would also be true if the cross plot were made at speeds other than 1000 rpm, because the different test runs shown in Figures 48 through 50 are essentially parallel.

The unsuccessful attempts to predict collector loss characteristics were based on analyses and correlations of completely flooded collectors and long annular gaps. The liquid-gas interfaces in the unflooded collectors are apparently of high significance. Two ways in which this interface could affect the collector losses are:

- The interface allows the cover gas to mix with the liquid metal in the current carrying gap.
- Liquid metal velocity profiles are altered near the interfaces.

Circumstantial evidence of the ingestion of gas into the liquid metal is available, even though it could not be observed directly in the experimental apparatus:

- It is known that in previously operated unflooded acyclic generators using NaK, foaming of the liquid has been a considerable problem at higher peripheral speeds.
- The open circuit loss data shown in Figure 46 indicates a falling off of torque at high-speed/high-field conditions. This effect could be explained by a gross decrease in the average gap fluid properties of density and viscosity caused by gas ingestion.

The axial nonuniformity of peripheral velocity and the presence of radial velocity components in the liquid metal in the vicinity of the gas interface, coupled with the magnetic field, cause electrical eddy currents to be generated. These velocity nonuniformities can be intensified by nonuniform transport current and the presence of gas in the liquid. Such eddy current losses might be expected to be proportional to the square of the intensity of the generated voltage and, indeed, the data shown in Figures 46 through 50 do indicate that the losses tend toward proportionality to $(BN)^2$ at the high levels of flux density and speed.

MOTORING TESTS

The test assembly was run as a motor by attaching a variable 2000-ampere power supply across the collector stators. The 25-hp motor previously used to drive the assembly was used as a loading mechanism. These tests were primarily qualitative in nature, noting the effects of motoring on liquid metal performance.

Observations relative to liquid metal performance led to the following conclusions:

- At the inner collector, the liquid metal tends to rotate in a direction opposite to the shaft rotation, particularly at low speeds. With the unit being run as a motor, current is fed through the disks in a magnetic field. As this current interacts with the axial component of the magnetic flux, tangential electromagnetic forces create the driving torque for the motor. In a disk-type machine, as tested, current flows in one direction (i.e., radially inward) through the smaller collector disk (inner collector) and then in the opposite direction (i.e., radially outward) in the outer collector. Because the current flows in different directions in the two disks in a constant magnetic field, the driving torques generated in the two disks are in opposite rotational directions. Due to the larger size of the outer collector, its driving torque is larger than that of the smaller collector, and it therefore becomes the driving force for the motor.

  The resulting motor output torque is a result of the difference between the two disk torques. The liquid metal in the inner collector gap sees the tangential electromagnetic force effects of the current flowing through it in the magnetic field. Therefore, while the inner disk turns in one direction, governed by the torque generated in the outer disk, the liquid metal in the inner collector gap tends to rotate in the opposite direction, due to the direction of the current flow through it. At low speeds, this results in spilling and splashing of the liquid at the inner collector disk gap.

  This general situation is similar to that which occured in the outer collector during previous testing when the unit was run as a generator. Due to the larger size of the outer disk, the direction of the generated current flow is determined by the rotation of this disk in the axial magnetic field. This generated current creates a reverse electromagnetic tangential force in the liquid metal in the gap. In the outer collector of the generator, therefore, the liquid tends to flow in a rotational direction opposite to the disk rotation. The ratio of electromagnetic forces to rotational drag forces (previously defined at δ) can be used as a guide to locate this occurrence in either the motor or the generator. When $\delta > 1$, the Lorentz forces

predominate and the liquid rotates accordingly. When $\delta < 1$, the drag forces of the disk predominate and the fluid rotates with the disk. As $\delta = 1$ is approached, neither effect is predominant and instability occurs.

- In the motoring tests, as the speed was increased the liquid did rotate with the disk as expected ($\delta < 1$).

- With increased magnetic field, other instabilities occurred at the rotor gap. At one setting, the entire liquid metal ring was thrust axially out of the gap and fell to the bottom of the cavity. This occurred intermittently at this setting. Another type of disturbance seen was the raining of gallium out of the gap around the entire periphery. Both of these types of disturbances occurred at relatively low speeds, high current settings, and high magnetic field strengths.

  These axial ejections of liquid from the gap are attributable to axial electromagnetic forces acting on the liquid. As the current flows in a closed loop through the rotor disks and stators, it generates its own magnetic field. With the interaction of the current with its own generated magnetic flux, an axial electromagnetic Lorentz force results. The effect of this force is to attempt to expel liquid from the collector gaps. It is this type of axial electromagnetic expulsion force that apparently caused the disturbances noted above.

- The expulsion effects could be stopped by increasing the speed or adding additional liquid. At higher speeds, or with increased mass, the centrifugal head developed by the fluid rotating at the side of the disk increases, creating a centrifugal pressure head to balance the expulsion pressure.

To simulate startup conditions, the rotor was locked, preventing rotation. The magnetic field strength and power supply current were then varied, and observations made:

- At any magnetic field strength setting, the liquid metal would start to rotate around the disk, due to tangential electromagnetic forces at low collector currents. As the current was increased, the gallium rotational speed increased. This verified the effects of the tangential electromagnetic force discussed above.

- When the current level reached a certain level, expulsion due to axial electromagnetic forces began (increased with the increased current), but eventually stopped at higher current levels. Evidently the axial electromagnetic force was not large enough to cause expulsion at low currents. As the current increased, so did both the tangential and axial electromagnetic forces. As a result, liquid rotation increased and expulsion began. As the current was further

increased, the centrifugal forces due to the rotation became large enough to counteract the expulsion forces, and expulsion stopped. The type of expulsion seen was the raining phenomena previously discussed.

- At higher magnetic fields, the axial expulsion stopped at lower current levels, due to higher peripheral velocities.

The collector configurations used in this test would not suffice for a liquid metal motor design. Prevention of liquid metal expulsion from the rotor gaps must be achieved before such a motor design could be practical. Additional baffles at the rotor tip, to direct flow spillage, flow bends, and other impedance to reduce expulsion effects and return loops to recirculate axially expelled fluid, are areas to consider in designing the collector disk configurations.

GENERAL TEST RESULTS

A period of three months elapsed from the initial charging of the test apparatus with gallium to the final teardown for inspection. During this time there were two major teardowns, during which the gallium was withdrawn into the bellows reservoirs and protected with cover gas. The liquid metal was not replaced; however, approximately 50 percent addition to the initial charge was made during the period, to replace liquid that was ejected from the collector gap to other cavities within the apparatus. A total of some 45 hours of running time was accumulated at speeds within the range of 400 to 2200 rpm, 35 hours of which were accumulated with the magnetic field applied at levels up to 6.5 tesla. The gallium filter system was valved off from the test apparatus during most of the running time, due to its interference with proper level regulation in the collector gaps. Nitrogen cover gas circulation was maintained at approximately 0.7 ft^3/hr during the entire time that the system was closed.

The apparatus was torn down for inspection at the end of this period. No evidence of a loss of liquidity or pasting of the gallium was evident in any part of the system, due to oxide formation. The appearance of the gallium on the peripheral surfaces of the disks and the matching surfaces of the collector stators had lost the uniform luster of the initial gallium electroplating and had taken on patchy grayness. However, the gray areas were still coated with gallium. The deterioration of these contact surfaces is compatible with the observed increase of internal resistance during the load testing. A probable contributing factor to the surface degrading is the arcing that took place across the gaps when load testing was done with insufficient liquid in the gaps; other investigators have not experienced this problem.

Gallium expands slightly when frozen. This expansion is a potential problem if the liquid metal freezes in enclosed spaces; however, no evidences of stress due to freezing were found.

The interior surfaces of the test apparatus were generally coated with a fine dusting of black powder. Microscopic examination of the dust showed it to be composed of extremely small spheres of gallium, the black color being caused by the small size of the spheres rather than their inherent color, which was metallic silver. The coating thickness on the transparent plastic part (part 12, Figure 35) was such that it only slightly reduced the light transmission, while the coating on a transparent plastic ring (part 5, Figure 43) encircling the shaft just inboard of the outer collector disk caused almost complete opacity. Testing the latter surfaces with a 500-volt megger produced no electrical reading, with the probes spaced about 0.1 inch apart. A small amount of the black powder was also found on the liquid metal filter disks.

Gallium spillover from the collector spaces was extensive, forming a pool about 3/4 inch high behind the observation window (part 28, Figure 35) and filling the housing nearly to the bottom of the shaft as far as the radial clearance seal (part 3, Figure 35) on the inside of the collectors. Extensive changes in the geometry of the baffles and guttering of the collectors is needed to control the liquid metal, but no evidence that this problem is peculiar to gallium (as opposed to NaK) exists.

The much thicker coating of dust in the inboard location is probably due to the shearing action of the radial clearance seal of the gallium that spilled over into this location (only 0.002-inch radial clearance between the seal and the shaft). A very thick deposit of the black powder existed on the bearing side of the radial clearance seal. Although a small amount of carbon worn from the seal ring may have been in this deposit, it was predominantly the finely divided gallium. No measurable wear was evident either on the inner base of the carbon ring or on the adjacent shaft surface, nor was any wear evident on the face seal that formed the primary atmospheric barrier.

CONCLUSIONS AND RECOMMENDATIONS

Following are the conclusions and recommendations resulting from the liquid metal current collector technology work:

- Losses in unflooded collectors more clearly approach a flux squared times speed squared $(BN)^2$ relationship than the cubic or higher power of speed relationship indicated by the investigations described in Reference 1.
- Gallium collectors can be successfully fabricated and operated using available materials and processes.
- Increases in the internal resistance of gallium liquid metal collectors during the period of the tests were noted. Similar increases were experienced in the tests, with NaK as the liquid metal -- as reported in Reference 1. More extended periods of testing and evaluation are required to isolate the causes and their long-term significance, if any.

- The particular shapes and collector configurations tested did not effectively confine the liquid gallium to individual collector sites. While this is of lesser significance for disk acyclic machines, it clearly indicates that further development would be required before gallium could be used in a multiple-drum superconducting acyclic machine.
- Inclination of the test rig to simulate propeller shaft inclination or ship pitch was only conducted for a single value of approximately 7 degrees. Further improvement in configuration to more effectively retain the liquid metal in the test site should be completed before any more extensive evaluation of pitch angles would be justified.
- Larger diameter collectors, more closely simulating mechanical and electrical configurations applicable to useful motor sizes and ratings, should be undertaken.

Appendix I

CURRENT COLLECTOR GAP LOSSES

The use of gallium as a collector fluid in place of NaK in a semiflooded system has the advantage of offering an inherent safety in the event of an accident. Due to the higher density and viscosity of gallium, one's first impression is that higher collector losses would occur. It can be shown, however, that in low-speed applications, such as those typical of ship propulsion motors, the use of gallium results in lower viscous losses.

In Reference 3, Equation 28, the average viscous loss in a radial collector gap is shown to be:

$$Pav = \frac{f\rho V_o^3}{8} \left[1 + 3\delta^2 \right] \qquad \delta > 1 \qquad (21)$$

$$Pav = \frac{f\rho V_o^3}{8} \left[2 (1 + \delta) \sqrt{2\delta - 1} \right] \qquad \delta > 1 \qquad (22)$$

where δ is a demensionless ratio relating the electromagnetic forces acting on the fluid to the viscous forces, specifically:

$$\delta = \frac{2JBd}{f\rho V_o^2}$$

f = Fanning friction factor

V_o = Collector peripheral velocity

ρ = Collector fluid density

J = Current density in collector gap

B = Magnetic flux density

d = Collector radial gap

The effect of fluid properties on the loss is not immediately evident from the above loss expressions. For various machines considered earlier in the study, it has been found that the typical values of δ are well above 1.0 for motors and are well below 1.0 for generators when NaK is assumed for a collector fluid. It is therefore instructive to simplify Equations 21 and 22, assuming extreme values of the dimensionless ratio δ:

$$Pav = \frac{f\rho V_o^3}{8} \qquad \delta << 1 \qquad (23)$$

$$Pav = \frac{(JBd)^{3/2}}{(f\rho)^{1/2}} \qquad \delta >> 1 \qquad (24)$$

It is seen from these equations that for low-speed machines ($\delta >> 1$), the collector loss varies inversely with the fluid density and thus the use

of gallium can improve the efficiency. This is due to the fact that in this condition, the fluid velocity is much higher than the collector peripheral velocity and it becomes the governing factor in the viscous loss. Increased density lowers this fluid velocity and hence lowers the losses. To give a concrete example of this, the propulsion motor presented in Table 43 of Reference 3 can be considered, where:

Power	=	40,000 hp
Inner collector radius	=	12.13 inches
Outer collector radius	=	18.53 inches
Magnetic flux density	=	5.0 Wb/m^2
Design current	=	150,000 amperes
Speed	=	200 rpm

At the inner and outer collectors, the dimensionless ratio, δ, has the following values when the collector fluid is NaK (density = 0.85×10^3 kg/m^3):

$$\delta_i = 22.9 \quad (25)$$

$$\delta_o = 18.2 \quad (26)$$

Assuming a radial clearance of 0.050 inch in both collectors, the inner and outer Reynolds numbers with NaK ($\mu = 4.7 \times 10^{-4}$ kg/ms) are:

$$(Re)_i = 29,600, \text{ therefore } fi = 0.0086$$

$$(Re)_o = 45,200, \text{ therefore } fo = 0.0085$$

where friction factors are obtained from Figure 8 of Reference 1.

If in this machine the NaK is replaced by gallium ($\rho = 6.0 \times 10^3$ kg/ms), the above parameters change to:

$$(Re)'_i = 65,400$$

$$(Re)'_o = 100,000$$

$$(fi)' = 0.0084$$

$$(fo)' = 0.0083$$

$$(\delta_i)' = 3.32$$

$$(\delta_o)' = 2.64$$

The ratio of NaK collector loss to gallium collector loss can be obtained from Equation 22:

$$\frac{\text{gallium loss}}{\text{NaK loss}} = \frac{f' \rho' (1 + \delta') \sqrt{2\delta' - 1}}{f \rho (1 + \delta) \sqrt{2\delta - 1}}$$

For the inner and outer collectors, these ratios become:

$$\left(\frac{\text{gallium loss}}{\text{NaK loss}}\right)_i = 0.44$$

$$\left(\frac{\text{gallium loss}}{\text{NaK loss}}\right)_o = 0.45$$

Thus for this illustrative case, the collector losses can be halved by the substitution of gallium for NaK.

Appendix II

REFERENCES

1. R.L. Rhodenizer, Development of Solid and/or Liquid Metal Collectors for Acyclic Machines, Final Report Task 4 & 5, Department of Defense Contract No. N00024-68-C-5415, Serial No. SF0130 702, Task 11582, General Electric Company, Schenectady, N.Y., 30 September 1971.

2. Cryogenic Systems and Superconductive Power, Second Semiannual Technical Report, Advanced Research Projects Agency Contract No. DAHC-15-72-C-0235, ARPA Order No. 2200, General Electric Company, Schenectady, N.Y., 1 October 1973.

3. R.L. Rhodenizer, Development of Solid and/or Liquid Metal Collectors for Acyclic Machines, Final Report (18 June 1968 to 31 December 1969), Department of Defense Contract No. N00024-68-C-5415, Serial No. SF0130 702, Task 11582, General Electric Company, Schenectady, N.Y., 27 February 1970.

4. R.H. Norris, et al., "Drag-Rotating; Cylinders Enclosed," Fluid Flow Design Data Book, Section G408-5, p. 2, General Electric Company, Schenectady, N.Y., 1969.

Preceding page blank